An Experimental Investigation of Heat Transfer to Hydrogen Peroxide in Microtubes

by

Mathieu Bernier

Submitted to the Department of Mechanical Engineering in
Partial Fulfillment of the Requirements for the Degree of

MASTER OF SCIENCE IN MECHANICAL ENGINEERING

at the

MASSACHUSETTS INSTITUTE OF TECHNOLOGY

June 2004

Author _____

Department of Mechanical Engineering
May 7, 2004

Certified by_____

Professor Alan H. Epstein
R.C. Maclaurin Professor of Aeronautics and Astronautics
Thesis Supervisor

Certified by _____

Professor Carol Livermore
SMA Assistant Professor of Manufacturing
Thesis Reader, Department of Mechanical Engineering

Accepted by _____

Professor Ain A. Sonin
Professor of Mechanical Engineering
Chairman, Committee on Graduate Students

An Experimental Investigation of Heat Transfer to Hydrogen Peroxide in Microtubes

by

Mathieu Bernier

Submitted to the Department of Mechanical Engineering on May 7, 2004
in Partial Fulfillment of the Requirements for the Degree of

MASTER OF SCIENCE IN MECHANICAL ENGINEERING

Abstract

Because of its strong oxidizing properties, high density, low-toxicity and environmentally friendly decomposition products, concentrated hydrogen peroxide has regained popularity as a propellant in many rocket applications. The MEMS-based MIT micro-rocket engine is one such application where 98% liquid hydrogen peroxide and JP7 are proposed as a propellant combination. Like other micro-thrusters concepts, the MIT micro-rocket engine uses its propellants to regeneratively cool the combustion chamber and the nozzle. Although JP7 has been proven to be an effective coolant under such conditions, hydrogen peroxide becomes unstable at high temperature and may explode, thus adding a critical constraint to the cooling scheme.

To address this issue, heat transfer experiments in 95 μm inside diameter, 4 mm long, electrically heated stainless steel microtubes have been performed to define the stability limit and explosion condition associated with 98% hydrogen peroxide thermal decomposition. Conditions such as pressures, temperatures, heat fluxes and length scale found in the engine were replicated. Tests were conducted whereby heat transfer to the hydrogen peroxide was increased until an explosion occurred. For each test, prior to the explosion, an experimental forced convective heat transfer coefficient has been obtained and compared to standard empirical correlations.

Experimental results indicate that 98% hydrogen peroxide has limited cooling capacity for a regeneratively-cooled rocket engine. Independent of pressure and mass flow, results show that a local fluid temperature of approximately 150°C consistently yields an explosion in stainless steel microtubes. In addition, standard macro-scale heat transfer correlations were found to significantly underestimate the heat transfer rates obtained experimentally. Instead, a correlation developed for forced convective heat transfer in microtubes is presented and provides a more accurate estimate.

Thesis Supervisor: Professor Alan H. Epstein
Title: R.C. Maclaurin Professor of Aeronautics and Astronautics

Acknowledgements

When I heard about MIT for the first time in 1997, I had never imagined that I would one day attend this institution and graduate from it. However, seven years later, here I am, as my advisor would say, "with the illusion of graduating in the near future" with a Master's degree. Although I have invested a lot of time and effort in this endeavor, it would not have been possible without the advice, friendship and help of many people. I would like to take this opportunity to specifically thank these people for their contribution and support.

First, I would like to thank my advisor, Prof. Alan Epstein, for the opportunity to work on the MIT micro-rocket engine project. Working under his supervision has been an invaluable experience. I would also like to extend my gratitude to Prof. Carol Livermore for kindly accepting to serve as a thesis reader and for proofreading this entire thesis so carefully. In addition, I would like to thank Prof. Jack Kerrebrock, Dr. Stuart Jacobson and Dr. Gerald Guenette for their guidance, support and dedication throughout this project. Their ability to listen to problems and their technical contribution were greatly appreciated.

James Letendre and Jack Costa also deserve a lot of credit for helping me with the design and building of the experimental test rig. Their time, competence, good humor and patience during testing (with the "ducky" suit) were greatly appreciated. I also want to thank the rest of the GTL staff, Julie Finn, Marie McDavitt, Holly Anderson, Susan Parker and Lori Martinez for consistently being in a good mood and for keeping a good social atmosphere in the laboratory.

I also owe a special thank to Chris Protz, my rocket-testing partner, for bringing me up to speed on the micro-rocket project, for answering my numerous questions and for providing general guidance on my project. In addition, I want to thank the remainder of the micro-rocket group, Shana Diez, Dr. Sun, Dr. Miki and Jin-Wook Lee for their technical support. It has been a pleasure working with all of you.

My time at the GTL would not have been the same without the many amazing people I have met here. Thanks to everyone at the GTL but especially to Josep, Partiv and my offices mates Lixian, Yiben, Caitlin, Emmanuel and Neil for helping me with classes, research and putting up with my constant habit of chatting and goofiness. Among those people, I would particularly like to thank Neil, for his good humor and his memorable quote on Navier-Stokes. I also which him good luck with his pursuit to conquer Formula One.

I could not end this acknowledgment section without mentioning and thanking my two long-time friends, Grant and Jean, who have embarked on this MIT journey with me, two years ago. To accurately describe how great it has been to share this experience with them would probably require a dissertation as thick as this thesis. So, let me limit myself by saying that the impact of their presence was incommensurable.

Almost finally, I would like to thank my parents and my sister for their love, support and encouragement. Despite the distance separating us, I always felt that you guys were right behind me. Finally, I would like to thank Andrea, for accepting to proofread this thesis and for supporting me on a daily basis, through good and rougher times. To say the least, my experience at MIT would not have been the same without you.

This work has been supported by DARPA, Dr. R. Rosenfeld, program manager. The support of this institution is also gratefully acknowledged.

Contents

List of Figures

List of Tables

Nomenclature

Acronyms

BLSF	Best Line Straight Fit
GTL	Gas Turbine Lab
HTP	High-Test Peroxide
IC	Integrated circuit
IR	Infrared
LOX	Liquid Oxygen
MEMS	Microelectromechanical Systems
SEM	Scanning Electron Microscope

Roman

A	surface area
A_i	inside surface area of the microtube
C	dimensional sensitivity of the uncertainty
Cp	specific heat
D	tube diameter
D_i	1/16″ tube inside diameter
D_o	1/16″ tube outside diameter
d_i	microtube inside diameter
d_o	microtube outside diameter
dx_i	dimensional uncertainty in x_i
$d\hat{y}$	derived dimensional uncertainty
dy	engineering uncertainty

E electric field

E_a activation energy

f friction factor

h heat transfer coefficient

I current

I_d density specific impulse

I_{sp} specific impulse

k thermal conductivity

L length of the microtube

L_{res} resistive length of the microtube

$\dot{m}$ mass flow

Nu Nusselt number

P pressure

P_{GEN} power generated from H_2O_2 decomposition

Pr Prandtl number

Q heat load or power

q heat flow

q'' heat flux

R resistance

r radial dimension (also radius)

Re Reynolds number

T temperature

T_{TANK} fluid temperature in the main tank

U mean fluid velocity

V voltage

x axial distance

x_i i^{th} sensor reading (measurement)

$\tilde{x}_i$ quantity with uncertainty

Greek

Δ	difference
σ	electrical conductivity
ρ	density or resistivity
μ	viscosity

Subscripts

b	bulk
c	critical
$_D$	diameter
$_{DISS}$	dissipated
f	film (also fluid)
i	inside wall conditions
in	entrance of the microtube
o	outside wall conditions
out	exit of the microtube
ss	exit of the microtube
$_{THEORY}$	theoretical quantity
$_{TOT}$	associated with the total assembly
$_{TUBE}$	associated with the microtube
w	wall

Chapter 1

Introduction

Microelectromechanical systems (MEMS) refer to the integration of mechanical elements, sensors, actuators and electronics on a common silicon substrate through microfabrication technology. While the electronics are fabricated using integrated circuit (IC) processes, the micro-mechanical components are fabricated using compatible micro-machining processes that selectively etch away parts of a silicon wafer [21]. Although only two-dimensional features are created at the wafer level, three-dimensional devices are fabricated by bonding together several extruded planar silicon wafers. First appearing two decades ago in the high-tech community [12], MEMS promises to revolutionize many products by integrating together microelectronics and micro-mechanical components, thus allowing the fabrication of complete systems-on-a-chip [21]. Because they can be batch manufactured like integrated circuits, MEMS devices have the potential for mass production and will most likely offer substantial cost saving in automotive, medical, and aeronautical weight-critical applications.

At MIT, a large effort has been dedicated to the study of MEMS for power and propulsion applications. In 1994, Epstein [7] initiated an effort at MIT's Gas Turbine Lab (GTL) to develop micro-gas turbine generators using MEMS technology. Made out of silicon, these millimeter- to centimeter-size heat engines are expected to produce useful power in the range of 10-100 W or 0.1-0.5 N of thrust in a few cubic centimeters [11]. In 1996, London [16] suggested that the micro-gas turbine technology could be adapted to realize high-pressure, turbopump fed, centimeter-sized rocket engines. Also made out of

silicon, these MEMS-based micro-rocket engines would use 300-s I_{sp} liquid propellants and produce about 15 N of thrust, thus yielding a thrust-to-weight ratio as high as 1000:1 [18]. Stationkeeping of satellites and micro launch vehicles are envisaged for such micro-rocket engines, which could be mass-produced and potentially reduce the cost of propulsion.

As part of MIT's MicroEngine project, this work studies the cooling properties of hydrogen peroxide as a potential propellant for future generations of the micro-rocket engine. In this chapter, after an overview of the micro-rocket engine project, a review of the propellant selection process is presented and the renewed interest for hydrogen peroxide is justified. This chapter ends by setting the objectives of the experimental heat transfer study and by briefly addressing the organization of the chapters presented in this thesis.

1.1 Overview of the Micro-Rocket Engine Project

1.1.1 Concept

The concept of MEMS-based chemical rocket engines for orbit maintenance and control was originally proposed by London [18]. These micro-rocket engines would be complete centimeter-sized liquid propulsion systems fabricated using semiconductor manufacturing technology and materials. Initial estimates suggest that such engines could produce thrust levels as high as 15 N using 300-s I_{sp} storable liquid propellants [18]. Having an integrated high-speed turbopump pressurizing system and a regeneratively-cooled system, these micro-rocket engines would eliminate the need for pressurized propellant tanks, thus lowering the mass of the overall system. Combined with the economic advantage of MEMS technology, liquid bipropellant micro-rocket engines present an attractive alternative to current micro pressure-fed propellant systems.

1.1.2 Cycle

Given the high level of geometrical complexity allowed by MEMS technology, a number of propulsion cycles were possible for a turbopump-pressurized, regeneratively-cooled liquid micro-rocket engine. Consequently, a detailed analysis was performed by Protz [26] and an expander pumping cycle was selected. Figure 1-1 shows the details of such an expander cycle for one of the two propellant feed lines.

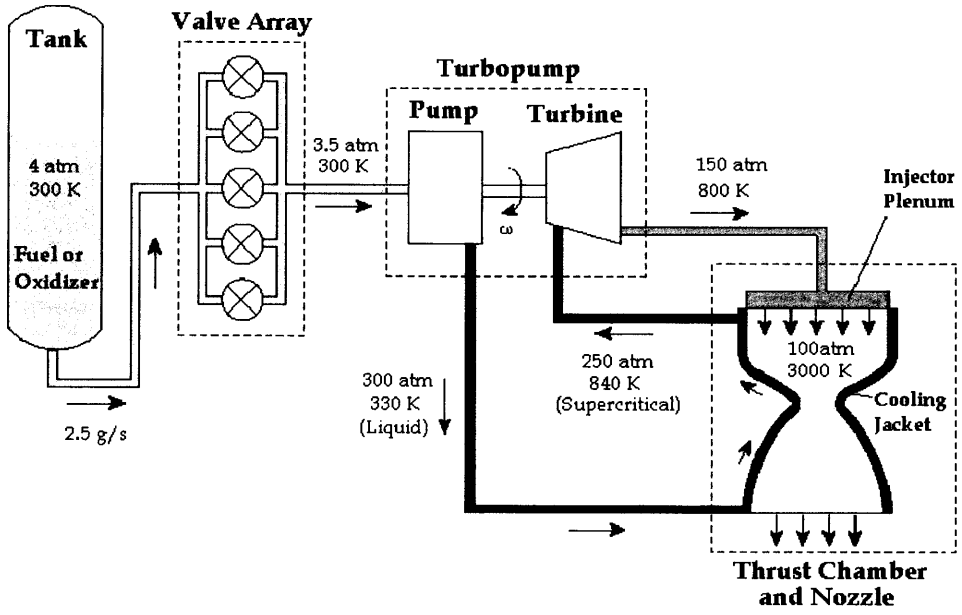

Figure 1-1: Intended expander cycle for the micro-rocket engine (only one propellant line shown) [Courtesy Dan Kirk, 2004].

As intended, the micro-rocket cycle uses two identical feed lines similar to the one shown in Figure 1-1. Each propellant, both the fuel and oxidizer, have their own feed tank, which is slightly pressurized. They also have their own set of valves and pumping system. As a result, the propellants do not mix until they pass through the injectors in the combustion chamber. The propellant mass flow is controlled by a set of valves, located downstream of the feed tanks. By opening in sequence, these valves control the oxidizer to fuel mass ratio and have a nominal 0-2.5 g/s mass flow modulation. Further downstream, each of the propellants flows through its own pump, which is driven by a

turbine. After the pump, the propellants pass through a cooling jacket around the rocket before entering the turbine. The purpose of this regenerative-cooling scheme is twofold: to cool the structure of the nozzle and thrust chamber, as well as to generate enough coolant enthalpy to drive the turbine. Finally, each of the hot propellants is expanded through a turbine before injection into the combustion chamber, where mixing occurs.

1.1.3 Components

Since the introduction of the concept in 1997, each of the main components of the micro-rocket engine propulsion system has been designed, built and tested. This section provides a brief summary of the thrust chamber, the turbopump and the valves development made to date.

Thrust Chamber and Nozzle

To evaluate the feasibility of micro-rocket engines, a proof-of-concept thrust chamber was designed, fabricated and tested by London [17]. For this device, gaseous oxygen and methane were selected as the propellants to minimize feed system complexity, and ethanol was used as the coolant. This device, which is 18 x 13.5 x 3 mm in size, is fabricated by bonding 6 etched silicon wafers, each 0.5 mm thick. As shown in Figure 1-2, 16 thrust chamber layers can be produced on a single wafer. Also shown in Figure 1-2 are the two halves of a complete thrust chamber with a combustion chamber, a nozzle, injectors and internal cooling passages [17]. Such a thrust chamber, further developed by Protz, has been operated up to a chamber pressure of 29.6 atm, with a thrust level of approximately 3 N [27].

Turbopump

As previously shown in Figure 1-1, the intended propulsion cycle requires a pressure of approximately 300 atm at the exit of the pump. In addition to high-pressure capability, the envisaged turbopump has the particularity of pumping propellants in liquid phase by use of supercritical, gaseous-like propellants in the turbine [12]. To assess the feasibility of such a turbopump, a demonstration 30 atm pressure-rise pump was

designed, fabricated and tested. Designed by Deux [6], this MEMS-based turbopump features pump blades and turbine blades on the same side of a 6 mm-diameter single wafer rotor, as shown by the scanning electron microscope (SEM) picture in Figure 1-3. Using air as the driving gas and water in the pump, tests to date have demonstrated a rotation speed of 114,000 rpm with a corresponding pressure rise of 9 psi [5].

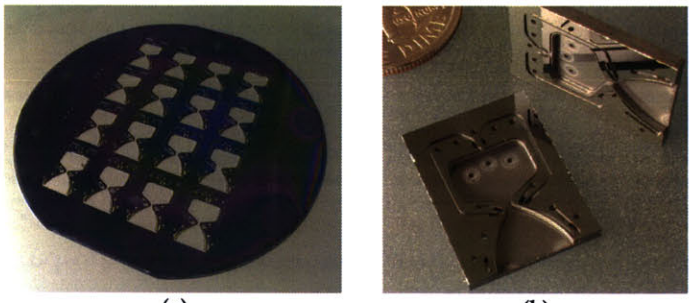

(a) (b)

Figure 1-2: Micro-rocket thrust chamber. (a) Sixteen identical layers of the micro-rocket thrust chamber on a 100 mm wafer [18]. (b) Two halves of micro-rocket thrust chamber and nozzle; nozzle exit is 7.5 mm wide [17].

Valves

To control the propellant mass flow, a MEMS-based two-stage valve concept was proposed. As intended, 5 of those two-stage valves, which include an electrostatic pilot valve and a servovalve, would modulate each of the propellant mass flows from 0 to a nominal 2.5 g/s. To evaluate the concept and reduce the technical risks, both components, the pilot valve and servovalve, were fabricated and tested separately. For the servovalve, test results generated by Kirk [13] showed proper functioning and actuation of the tether-supported boss, shown in Figure 1-3. The concept of an electrostatic pilot valve was confirmed experimentally by Lee [14]. For such a device, significant flow modulation was achieved in spite of an observed valve displacement that was only 55% of design. Both valve components are still under development and will be tested in series in the near future.

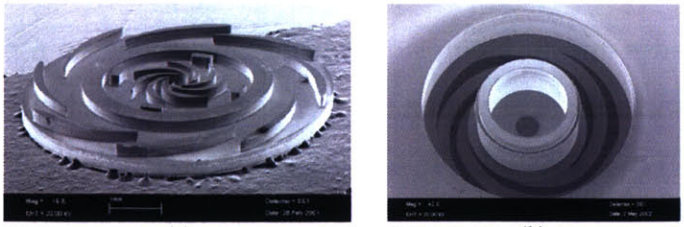

(a) (b)

Figure 1-3: SEM pictures of micro-rocket engine system components. (a) Turbopump rotor 6 mm in overall diameter [6]. (b) Moving component of the servovalve 2.5 mm in overall diameter [Courtesy Jin-Wook Lee, 2004].

1.1.4 System Integration and Future Generations of Micro-Rocket Engines

As previously mentioned, the intent of the micro-rocket engine project is to build a complete, regeneratively-cooled, turbopump-pressurized propulsion system using storable liquid propellants. Ultimately, after proper redesign and maturation, the engine components presented above will be combined with their power electronics, and integrated on a single silicon chip using microfabrication technology. Figure 1-4 shows a conceptual drawing for a propulsion-system-on-a-chip, estimated to be 18 x 14 x 5 mm [11].

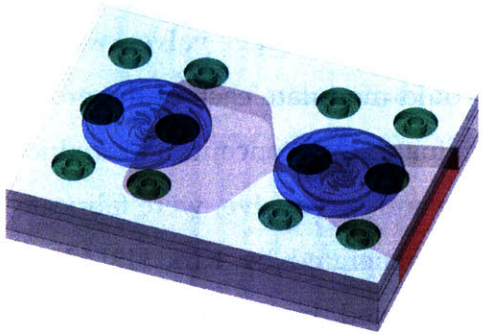

Figure 1-4: System-on-a-chip conceptual drawing of the micro-rocket engine [Courtesy Stuart Jacobson, 2004].

Prior to this integration, the proof-of-concept thrust chamber, the injectors and the cooling passages need to be redesigned to represent the actual expander cycle, which will use liquid propellants and a regenerative cooling scheme. Although an expander cycle is a proven way to pressurize propellants [30], one major uncertainty in the current

system remains and needs to be addressed. Because the pumping system is ultimately coupled with the regenerative-cooling scheme, the success of the cycle is highly dependent on the cooling properties of the propellants. To mitigate this uncertainty, various propellants have been investigated, both theoretically and experimentally, with a particular emphasis on their cooling properties. The coming sections review the work that has been done in this area, and justify the experimental hydrogen peroxide study that will be presented in this thesis.

1.2 Previous Work on Propellant Analysis

Concurrent to the testing and development of the micro-rocket components, several propellant combinations were investigated for the overall propulsion system. First, Al-Midani [1] performed a preliminary study using liquid oxygen (LOX) and ethanol as propellants. Then, Protz [26] expanded this work by examining cycles suitable for storable propellants. On the basis of their performance (I_{sp}, I_d), toxicity, handling, storage and cooling properties, JP7 and hydrogen peroxide were selected as candiate propellants for the liquid micro-rocket engine. Despite yielding a lower performance (315 s Isp) than a nitrogen tetroxide/hydrazine (N_2O_4/N_2H_4) propellant combination (322 s Isp), JP7 and hydrogen peroxide were identified as offering a non-toxic, environmentally friendly, and easier to handle combination [26]. Following the ethanol and water heat transfer studies performed by Lopata [19] and Faust [8], Joppin [12] studied the cooling properties of JP7 in micro-channels at heat fluxes, pressures, and length scale relevant to the design of the micro-rocket. From her study, Joppin experimentally determined that JP7 has sufficient stability and heat capacity to serve as a fuel for the regeneratively-cooled micro-rocket engine [12].

1.3 Motivation and Objectives

The suitability of hydrogen peroxide as an oxidizer for the micro-rocket engine has not been established experimentally. Although it has been used extensively in recent years due to its low-toxicity and clean decomposition products, concentrated hydrogen

peroxide presents some stability problems at high temperature and may explode, thus adding a critical constraint to the cooling scheme. Because of the high heat fluxes and temperatures envisaged, this constraint might jeopardize the use of hydrogen peroxide in the micro-rocket engine.

Consequently, the work presented in this thesis aims to determine the suitability of concentrated liquid hydrogen peroxide as a propellant for the regeneratively-cooled, turbopump-pressurized, liquid micro-rocket engine. Following the framework established by Joppin [12], heat transfer experiments to hydrogen peroxide in microtubes are performed with the following two objectives:

- To determine the onset of decomposition instability (explosion) in a hydrogen peroxide cooling passage, at high pressures and high heat fluxes.
- To estimate the heat transfer properties of hydrogen peroxide in micro-channels at heat fluxes, pressures and mass flows relevant to the design of the micro-rocket engine.

Taken together, the fulfillment of these two objectives should allow a clear conclusion concerning the suitability of hydrogen peroxide for future generations of micro-rocket engines.

1.4 Thesis Organization

This first chapter has introduced the concept of micro-rocket engines and has reviewed the previous work done on propellant analysis. In the same vein, it has motivated the hydrogen peroxide coolant study and set the objectives for the heat transfer experiments in microtubes. Chapter 2 introduces hydrogen peroxide and provides background information necessary for the understanding of subsequent chapters. Chapter 3 describes the principles of the heat transfer experiment, the experimental apparatus and the data reduction procedure. Chapter 4 presents and discusses the results obtained

from the heat transfer tests performed with 98% hydrogen peroxide. The final chapter summarizes the work presented in this thesis, addresses the impact of the results on future designs of the micro-rocket engine and gives some recommendations for future work.

Chapter 2

Hydrogen Peroxide

High concentration liquid hydrogen peroxide has been proposed as a propellant in combination with JP7 for the regeneratively-cooled MIT micro-rocket engine. Accordingly, after a short introduction, this chapter reviews the use of hydrogen peroxide in rocket applications. Then, the thermo-physical properties of concentrated hydrogen peroxide are presented as well as the decomposition reaction, safety, handling and material compatibility, all of which are crucial in the understanding of subsequent chapters.

2.1 Introduction to High Concentration Hydrogen Peroxide

Hydrogen peroxide, represented by the chemical formula H_2O_2, was discovered by Thenard in 1818 [28]. At ambient conditions, it is a clear, colorless, water-like liquid, heavier and slightly more viscous than water. It is a strong oxidizer with the unusual characteristic of being able to decompose exothermically into water and oxygen [31]. Because it is miscible in all proportions with water, hydrogen peroxide is most often found and used in aqueous solutions. At low concentrations, it is used as a bleaching agent for the pulp and paper industry. At high concentrations, that is, solution containing over 70% by weight of hydrogen peroxide, it is used for industrial and military purposes [29]. Such solutions, for which hydrogen peroxide concentration is above 70%, are commonly referred to as High-Test Peroxide (HTP). Rocket grade hydrogen peroxide, with a concentration varying from 70% to 98%, falls into the HTP category.

2.2 Use of Concentrated Hydrogen Peroxide in Rocket Applications

2.2.1 Brief History of Hydrogen Peroxide Rocket Development

The use of high concentration hydrogen peroxide for power generation and rocket application is quite common. In fact, its military potential has been recognized by the US Navy as early as 1933 [29]. However, most the early work on hydrogen peroxide propulsion was done in Germany, before and during World War II [3]. In 1936, Helmut Walter's hydrogen peroxide engine was chosen to propel the Heinkel He 176 aircraft. This first monopropellant engine used cold hydrogen peroxide of concentration 80% and a calcium permanganate solution as a catalyst to enhance decomposition [3]. Shortly after this, Walter developed a second engine, this time using 30% hydrazine and 80% hydrogen peroxide as an oxidizer [3]. This engine, which can be categorized as a hot bipropellant rocket engine, made use of the hypergolic (self-igniting) characteristics of this fuel-oxidizer mixture and thus did not require additional catalyst. These two engines were pioneers to what is perhaps the most well known application of HTP during World War II: the V2-rocket turbo-pump gas generator [3,31].

After World War II, the interest in hydrogen peroxide's compact energy potential and strong oxidizing properties triggered several research projects in the United States, Britain and the Soviet Union [3]. Some of the applications investigated at the time include: auxiliary power units for aircraft, torpedoes and submarines, rocket booster systems for helicopters, liquid explosives, and advanced rocket propulsion systems for aircraft and space vehicles [29]. Examples such as the English Black Knight/Black Arrow launch platform and the US X-15 rocket research plane are among the applications developed at that time.

After a period of rapid emergence, hydrogen peroxide became obsolete in both aircraft and space propulsion [3]. The jet engine replaced hydrogen peroxide in the aviation sector, whereas substances yielding higher specific impulse like hydrazine (N_2H_4), nitrogen tetroxide (N_2O_4) and liquid oxygen (LOX) replaced hydrogen peroxide in space

applications. As a result, HTP was temporarily abandoned for rocket propulsion, and regular production of rocket grade hydrogen peroxide was stopped in the US in the mid 1980's [3].

Despite early-improved performance, new space propulsion systems using N_2H_4, N_2O_4 or LOX were poisonous, carcinogenic and harmful to the environment. In addition, they were often more complicated and more expensive than their hydrogen peroxide predecessors [3]. In the 1990's, as environmental concerns became a priority, hydrogen peroxide received renewed interest mainly because of its environmentally friendly decomposition products, its handling simplicity and its lower cost. After a decade of intensive research, hydrogen peroxide is more than ever considered as an attractive choice for rocket propulsion [31].

2.2.2 Attractive Features of Concentrated Hydrogen Peroxide [31]

The following section presents in more detail the attractive features of hydrogen peroxide for modern rocket propulsion.

Reasonable performance as a monopropellant

High concentration hydrogen peroxide can be used as a monopropellant by taking advantage of its exothermic decomposition reaction into water and oxygen. Historically, this reaction has been achieved by flowing hydrogen peroxide through a silver or platinum catalyst screen. The vacuum specific impulse (I_{sp}) of 100% hydrogen peroxide is approximately 190 s [1], when used as a monopropellant. For comparison, under the same conditions[1], hydrazine yields an I_{sp} of 240 s .

Strong liquid oxidizer

Concentrated hydrogen peroxide can be used as the oxidizer in a liquid bipropellant system [30,31]. Even though it has strong oxidizing properties, concentrated hydrogen

[1] Chamber pressure = 500psia, shifting equilibrium, expansion ratio = 100 [31].

peroxide yields slightly lower performance than LOX or N_2O_4, when combined with liquid fuels. As an example, under the same conditions, the propellant combinations 90%H_2O_2/RP-1 [2] yields a theoretical specific impulse of 297 s [3] whereas the combination LOX/RP-1 yields an I_{sp} of 300 s [3] [30].

High density

The density of 100% hydrogen peroxide is 1442.2 kg/m^3 at room temperature. This is comparable to nitrogen tetroxide (1447 kg/m^3) and is higher than liquid oxygen (1140 kg/m^3). This is a desirable feature for rocket propulsion because it lowers the volume and the dry mass of the oxidizer tanks [30].

High specific heat

At 2650 J/kg-K, hydrogen peroxide has a high specific heat, similar to that of nitrogen tetroxide. Accordingly, it has been used to regeneratively cool the thrust chamber in pump fed rocket engines such as the Rocketdyne AR2-3 and the Reaction Motors LR-40 [31].

Storable

Historically, hydrogen peroxide has been abandoned partly because of its long-term storage stability. However, considerable improvements over the last decade in stabilizing additives and container materials have made hydrogen peroxide attractive again for long-term storage. In a properly designed container, hydrogen peroxide can be stored for extended periods with an acheivable decomposition rate lower than 1% per year [10].

Low-toxicity

Hydrogen peroxide is considered non-toxic because its effects on humans are considerably less than other propellants like nitrogen tetroxide, nictric acid (HNO_3) and

---

[2] RP-1 is highly refined kerosene; RP stands for refined petroleum [30].

[3] Chamber pressure = 1000 psia, exit pressure=14.7 psia, optimum expansion, frozen chemistry [30].

hydrazine, which are either toxic, poisonous or carcinogenic. In addition, because of its low vapor pressure, an open container of hydrogen peroxide does not produce a large amount of vapor. As a result, inhaling hydrogen peroxide vapor does not represent a health concern under normal workday exposures [33].

Clean decomposition products

As mentioned before, hydrogen peroxide can be exothermically decomposed into water and oxygen, which are benign substances to the environment. Consequently, there has been renewed interest in using hydrogen peroxide in propulsion systems because it yields non-toxic decomposition products.

Hypergolic with certain fuels

Hydrogen peroxide has the potential to be hypergolic (self-igniting) when brought in contact with certain fuels. This is a desirable feature because it eliminates the ignition system and greatly simplifies the overall propulsion system [30]. Helmut Walter was the first one to recognize this benefit of hydrogen peroxide and implemented it in his second engine, which used a hypergolic $85\%H_2O_2/30\%N_2H_4$ propellant combination [3]. See reference [20] for a complete list of hypergolic fuels with hydrogen peroxide.

2.3 Thermo-Physical Properties

Heat transfer tests have been done with 98% hydrogen peroxide[4] to estimate the heat transfer and the thermal stability limit at conditions close to those experienced in the micro-rocket engine. In order to reduce the data and predict the heat transfer coefficient, thermo-physical properties of 98% hydrogen peroxide such as density, viscosity, specific heat and thermal conductivity were required at high pressures and high temperatures. Unfortunately, no data at those conditions was found in the literature for 98% liquid hydrogen peroxide. Consequently, calculations were made based on the properties of

[4] The high concentration rocket grade hydrogen peroxide used in this thesis was supplied by FMC Corporation (Hydrogen Peroxide Division) in 1gallon glass bottles. As per FMC specifications, the concentration obtained varied from 98% to 99% and the 24-hour storage stability was approximately 99.5%.

HTP found at atmospheric pressures and moderate temperatures from the FMC Chemicals Technical bulletin number 67 [9]. This section tabulates, in SI units, the thermo-physical properties of 98% hydrogen peroxide used in this thesis.

2.3.1 Density

The density of 98% liquid hydrogen peroxide at 1 atm is shown in Table 2-1 for different temperatures.

Temperature [°C]	Density [kg/m^3]
0	1459.4
25	1430.9
50	1402.4
96	1347*

*extrapolated value [9]

Table 2-1: Density of 98% liquid hydrogen peroxide at 1 atm [9].

2.3.2 Viscosity

The viscosity of 98% liquid hydrogen peroxide at 1 atm is shown in Table 2-2 for different temperatures.

Temperature [°C]	Viscosity [10^{-3} Ns/m^2]
0	1.810
25	1.156
50	0.815
80	0.632*

*estimated by Protz [27]

Table 2-2: Viscosity of 98% liquid hydrogen peroxide at 1 atm [9].

2.3.3 Specific Heat

The mean specific heat of 98% liquid hydrogen peroxide between 0°C and 26.9°C is 2650 J/kg-K [9]. Due to the lack of data available, this specific heat has been assumed to be constant for temperatures above 26.9°C. In general, this assumption holds for most liquids over a small temperature range. As an example, the specific heat of water varies by a maximum of 2% from 0 to 150°C [15].

2.3.4 Thermal Conductivity

The thermal conductivity of 98% liquid hydrogen peroxide at 1 atm is shown in Table 2-3 for different temperatures.

Temperature [°C]	Thermal Conductivity [W/m-K]
0	0.555
25	0.587
80	0.657*

*extrapolated value [9]

Table 2-3: Thermal conductivity of 98% liquid hydrogen peroxide [9].

2.3.5 Boiling Point

The boiling point of 98% liquid hydrogen peroxide at 1 atm is 149.4°C [9].

2.3.6 Freezing Point

The freezing point of 98% liquid hydrogen peroxide at 1 atm is -1.5°C [9].

2.3.7 Critical Point

The critical conditions for pure liquid hydrogen peroxide are $P_c = 214$ atm and $T_c = 457$°C [9].

2.4 Decomposition Reaction

Pure isolated hydrogen peroxide is quite stable. However, many factors such as contaminants, catalysts and heat can disrupt this stability and induce its decomposition. Independent of their source, all those decomposition reactions are alike [22] and the overall process can written as:

$$H_2O_{2\,(l)} \xrightarrow{k} H_2O_{(l)} + \tfrac{1}{2} O_{2\,(g)} + \text{energy} \qquad (2.1)$$

At 25°C and 1 atm, this decomposition process liberates energy at a rate of 2884.5 kJ/kg with a corresponding adiabatic decomposition temperature of approximately 996°C [9].

Although all hydrogen peroxide decomposition processes obey equation 2.1, many factors influence the rate at which the reaction occurs. Among those factors, solution activity, surface activity and temperature [29] are considered the major drivers and will be discussed in the following sub-sections. Special attention will be given to temperature effects, due to their relevance to the current experimental investigation.

2.4.1 Solution Activity

Various metallic ions such as Cu^{++}, Fe^{+++} and Cr^{+++} are known to catalyze the decomposition of hydrogen peroxide [29]. For highly concentrated solutions, the amount of metallic ions dissolved is carefully controlled by manufacturers and stabilizers are often added to reduce their effect on the decomposition process.

2.4.2 Surface Activity

The rate of decomposition is very susceptible to surface activity. In general, most of the usual construction materials such as steel, copper alloys and magnesium alloys have catalytic effects on the decomposition of hydrogen peroxide. Other materials such as borosilicate glass (Pyrex®), pure aluminum, stainless steels of the 300 series and some polymers have low surface activity [29]. Even under the best storing conditions in a Pyrex® container, hydrogen peroxide is known to decompose at a rate of 1% per year [10]. Experiments have shown that surface treatments such as passivation and annealing can significantly improve the stability of hydrogen peroxide. This suggests that by itself, hydrogen peroxide is stable, but that any interface with another material, will tend to reduce its stability.

2.4.3 Temperature Effects

2.4.3.1 Thermal Decomposition

It is well known that an increase in temperature considerably increases the rate of decomposition of hydrogen peroxide [22,25,33]. As rule of thumb, the hydrogen peroxide safety documentation states that the decomposition rate increases twofold for each 10°C rise in temperature in the 20°C-100°C range [29]. Because of this increasing

reaction rate, thermally induced hydrogen peroxide decomposition often leads to uncontrolled chain reactions. To get a feel for the temperatures and reaction rates involved, Figure 2-1 shows the power (in the form of heat) generated in the liquid phase as a function of liquid temperature, for two different concentrations. From the shape of the curve, the exponential effect of temperature on the heat generated by decomposition is clearly noticeable.

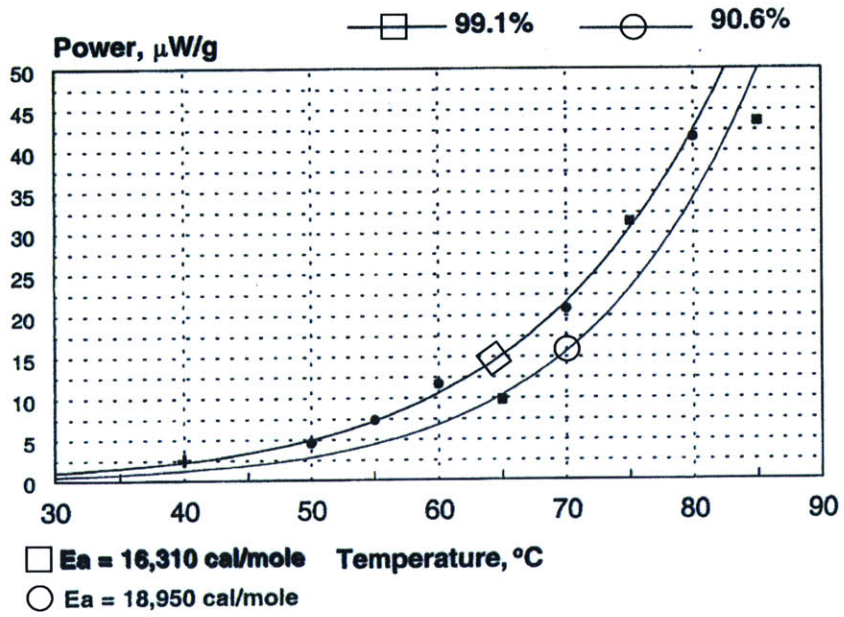

Figure 2-1: Power generated from the decomposition of hydrogen peroxide vs. temperature [25].

To further understand the effect of temperature on reaction rate, the experimental data presented in Figure 2-1 can be fitted using an equation of the Arrhenius form. Accordingly, the power generated at any temperature can be calculated as follows [25]:

$$P_{GEN} = B\exp\left[\frac{-E_a}{RT}\right] \tag{2.2}$$

where P_{GEN} is the power generated in kW/kg, B is a constant equal to $5.272\text{x}10^5$ kW/kg, E_a is the activation energy obtained experimentally at 16,310 cal/mole, R is a property of

hydrogen peroxide equal to 1.987 cal/mole-K and T is the temperature in degree K.

From equation 2.2 the effect of the various decomposition contributors become clear. For example, an increase in temperature will increase the decomposition rate exponentially. Also, surfaces with higher activity, which lower the activation energy, will tend to increase the speed of the reaction.

2.4.3.2 Vapor Explosions

High purity hydrogen peroxide solutions are not considered to be explosive hazards [29]. However, at atmospheric pressure, hydrogen peroxide vapor in concentration above 26 mol% (40 weight %) becomes explosive in a temperature range near the boiling point [22,29,34]. This characteristic of hydrogen peroxide is shown graphically in Figure 2-2. The shaded area is bounded on top by the boiling curve at 1atm and at the bottom by experimental vapor explosion data. In this region, known to be hazardous to explosions, the hydrogen peroxide vapor concentration is above 26 mol%. It is also important to note that the parabolic-shape curve in Figure 2-2 represents the locus of all liquid phase concentrations which yield a vapor concentration of 26 mol%. To the left of

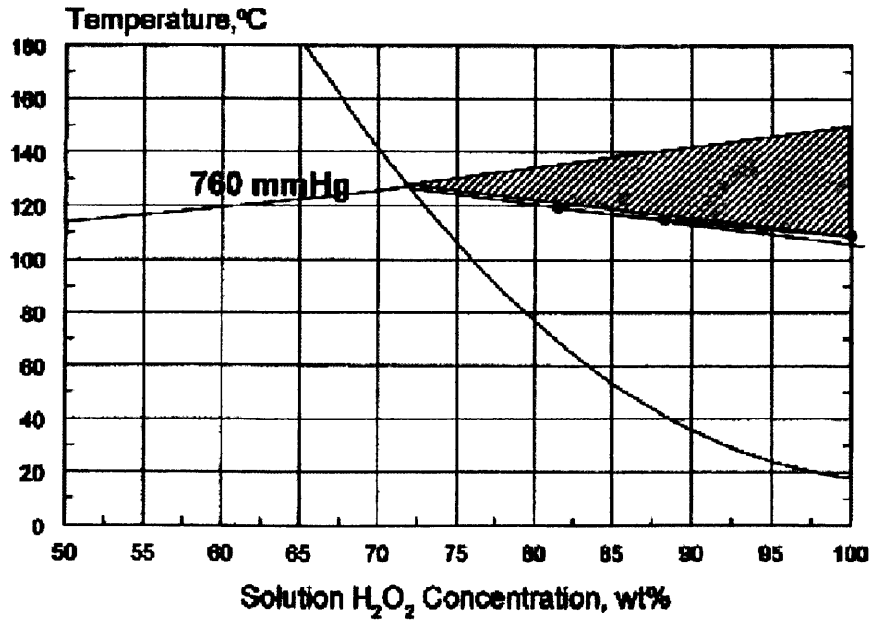

Figure 2-2: Hydrogen peroxide vapor explosive region at 1atm (shaded region)[34].

this curve, critical vapor concentrations are never achieved and vapor explosions are prevented. At atmospheric pressure, this corresponds to a liquid hydrogen peroxide concentration of about 73%.

Because it is bounded by the boiling curve, it is not surprising that the shape of the vapor explosive region depends on pressure. As a result, for 98% liquid hydrogen peroxide, the lower limit on vapor explosion temperature rises from a nominal 110°C for 1 atm, to 126°C for a pressure of 2 atm. The actual shape of the vapor explosive region is shown in Figure 2-3 for moderate pressures.

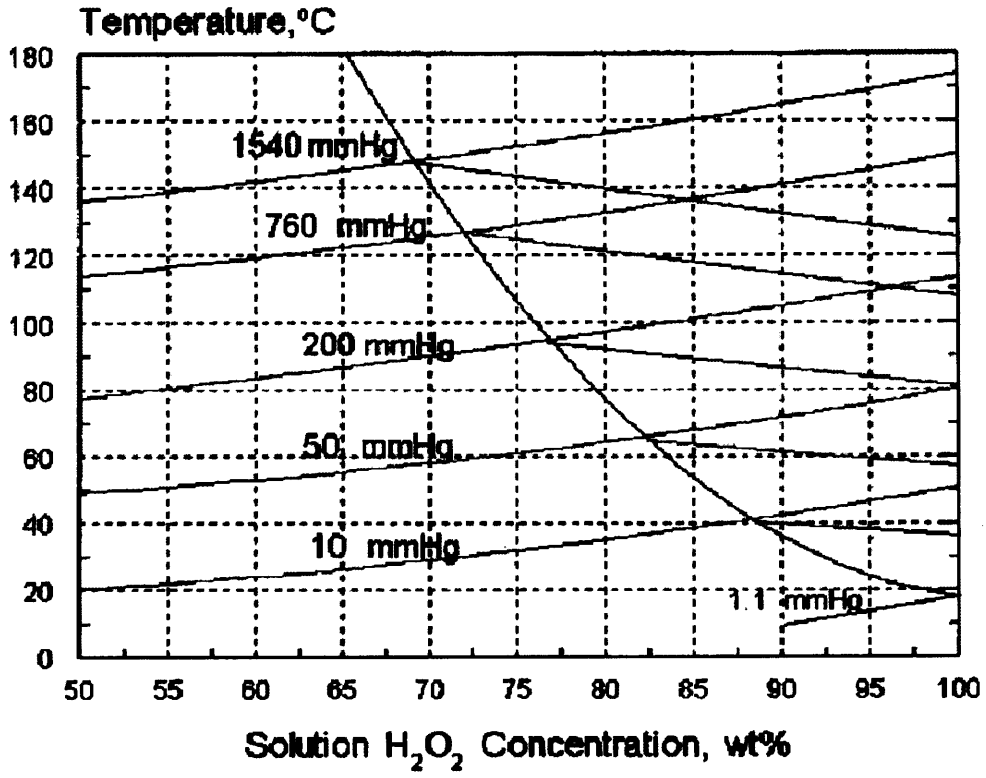

Figure 2-3: Effect of pressure on hydrogen peroxide vapor explosive region (regions not shaded here) [34].

From the above discussion, it should become apparent that there are limitations in using concentrated hydrogen peroxide as a coolant for rocket nozzles. Despite the high pressures involved, the thermally induced decomposition reaction could cause very

high local heating rates, which in turn could produce vapor in high enough concentration to lie in the explosive region. Although this process has been known for years, very little research has been directed at understanding and determining the limits for hydrogen peroxide vapor explosion under high temperatures and pressures, typical of rocket nozzle cooling passages.

2.5 Safety and Handling

Due to its strong oxidizing properties, its decomposition reaction and its potential for vapor phase explosion, hydrogen peroxide represents a health and safety hazard. Accordingly, great care must be taken when handling and storing hydrogen peroxide. The following sub-sections provide a brief overview into the safety and handling of concentrated hydrogen peroxide.

2.5.1 Health Hazard

Hydrogen peroxide is non-toxic. Nevertheless, inhalation of hydrogen peroxide vapors can cause irritation and inflammation of the respiratory tract. However, in a well-ventilated area, an open container of hydrogen peroxide does not produce enough vapors to represent a great health concern [33]. Perhaps a greater hazard of hydrogen peroxide to the human body is the risk of injury by contact with the skin, the eyes or the danger of burns caused by ignition of clothing [29]. Consequently, proper attire is required when handling hydrogen peroxide. Ordinary fabrics such as cotton, wool and leather should be avoided. Instead, permeable clothing made of Dacron, Dynel or Orlon is suggested [10,29]. For full body protection, clothing made of Koroseal or Neoprene should be used. In addition, for most common operations, complete attire requires safety goggles and facial masks as well as Neoprene aprons, gloves and boots. In case of a spill, all clothing must be thoroughly flushed with water. For a more detailed treatment of hydrogen peroxide heath hazards, see references [9], [10] and [29].

2.5.2 Decomposition / Explosion Hazard

By itself, concentrated liquid hydrogen peroxide is non-explosive and non-inflammable. However, in contact with any organics it may decompose, ignite or produce explosive mixtures [29]. Great care must be taken in preventing contamination with foreign particles during handling, storage and disposal. Another potential hazard of hydrogen peroxide is its susceptibility to detonation [34]. Despite the apparent insensitivity of the liquid phase, studies have demonstrated the hydrogen peroxide vapor phase to be sensitive to detonation by shock and impacts.

2.5.3 Handling

Small quantities of concentrated hydrogen peroxide can successfully handled in a lab environment, provided proper training of the personnel and adequately designed equipment. As a general rule, hydrogen peroxide should never be confined [29]. It should be stored in its original container, in a temperature-controlled environment. In addition, relief mechanisms should be added to the container to avoid dangerous oxygen pressurization. Due to its low vapor pressure [9], hydrogen peroxide can also be poured safely between open containers. As will be presented in the next section, all glassware and experimental equipment must be properly passivated to avoid contamination. During all operations, a supply of deionized water should be readily available. In case of accident, hydrogen peroxide spills and fires should be neutralized with large amounts of water. In emergency situations, the effects of water are twofold: it absorbs the heat released by decomposition and reduces the concentration of the solution [34].

According to FMC's safety manual, handling of concentrated hydrogen peroxide can be summarized in four simple rules [33]:

- Never contaminate
- Never confine
- Never contact
- Always have water available

2.6 Material Compatibility

Concentrated hydrogen peroxide presents some compatibility issues with most of the usual construction materials because of its strong oxidizing properties. In general, heavy metals such as lead, iron, manganese, cobalt, silver, gold, platinum and others catalyze hydrogen peroxide [10]. Some of the recommended materials for use with concentrated hydrogen peroxide are borosilicate glass (Pyrex®), high purity aluminum, stainless steel alloy 304 and 316, and polymers such as polytetrafluoroethylene (PTFE or Teflon®) and fluorocarbon (FKM or Viton®). Despite their quoted compatibility, all those materials destabilize hydrogen peroxide to some extent due to their surface activity. As a result, four material compatibility classes have been established based on the rate of decomposition (oxygen loss) that they induce. Table 2-4 presents these classes as well as corresponding examples [10].

	Definition	Examples
CLASS 1	Satisfactory for unrestricted use	Zirconium, Aluminum 1060 & 5254, Pyrex®, Teflon®, Viton®
CLASS 2	Satisfactory for repeated short time contact (4 hours at 72°C or 1 week at 22°C)	Stainless Steel 304 & 316, Silicon, Silicon carbide, Tin, Fluorolube, some PVC's, Polyethylene
CLASS 3	Only for short-time contact (1 min at 72°C or 1hour at 22°C)	Stainless Steel 17-4 ph, Inconel X, Tygon, Nickel, Silicone
CLASS 4	Not recommended	Silver, Lead, Cobalt, Platinum, Copper, Iron, Gold, Titanium, Zinc, Graphite,

Table 2-4: Hydrogen peroxide compatibility classes for various materials [10].

As can be seen from the short compatibility list presented in Table 2-4, using hydrogen peroxide in a test rig may present some compatibility problems. However, safe design and operation of the rig is possible provided adequate material selection and passivation. The following sub-sections briefly address the impact of compatibility on parts selection and provide guidelines into the passivation process.

2.6.1 Impact on Parts Selection

When designing a test rig for concentrated hydrogen peroxide, all parts should be made of class 1 or class 2 materials [10]. For the entire rig, knowledge of every part's composition is required. To ensure safe operation of the rig, parts such as tubing, valves, pressure transducers, flowmeters, o-rings, seals, lubricating oil, coating and others, should be investigated or tested for compatibility. As a general rule, if the compatibility of a given material is unknown, chances are that it is not compatible. Although most of the details are left out here, reference [10] presents a detailed list of compatible materials with concentrated hydrogen peroxide.

Selecting parts to be used with hydrogen peroxide can be a complex problem. Unfortunately, it has been found that most suppliers have no information about their product's compatibility with concentrated hydrogen peroxide. For the test rig presented in the coming chapter, many compatible parts were found off the shelf, under special order or provided small modifications. A list of parts used in the current test rig, which have been found to be compatible with hydrogen peroxide, is included in Appendix C.

2.6.2 Passivation

Before compatible parts can be used in a HTP system, they need to cleaned for hydrogen peroxide service and passivated. The American Society for the Testing of Materials [2] defines passivation as "the removal of exogenous iron or iron compounds from the surface of stainless steel by means of a chemical dissolution with an acid solution that will remove the surface contamination". In the case of hydrogen peroxide passivation, the removal of contaminants or ions reduces the surface activity of a given material and increases its stability.

Depending on the type of material passivated, the procedure may vary[5]. In general, for stainless steels components, after a thorough degreasing, the part is typically submerged

[5] See reference [10] for a complete material-specific treatment of passivation procedures.

in 70% nitric acid. As reported in reference [4], 15 min immersion in acid was found to be sufficient for stainless steel passivation. Nominal immersion periods of 2 hours, suggested by industry standards, were found to cause galling of threads and were thus shortened. Following the acid immersion, a protective passive film is formed on the part, by conditioning it with 30% hydrogen peroxide. After this sequence and a thorough deionized water flush, the part is considered ready for use with concentrated hydrogen peroxide.

Simple components such as tubing can be passivated according to the procedure described above. However, for components such as valves and transducers, industry standards suggest disassembling them into their respective components and passivating them separately. Appendix D provides a successful passivation procedure developed for the type of valve used on the current test rig.

2.7 Summary

This chapter has provided the background information on hydrogen peroxide necessary for the understanding of subsequent chapters. After a brief historical review of HTP rockets, the attractive features of concentrated hydrogen peroxide were presented. In addition, this chapter reviewed the thermo-physical properties of 98% hydrogen peroxide, described its thermal decomposition reaction and presented the relevant safety, handling and material compatibility. The next chapter will describe in detail the experimental apparatus with which the 98% hydrogen peroxide heat transfer tests have been performed.

Chapter 3

Description of the Experiment

A heat transfer experiment has been designed and built to test hydrogen peroxide in microtubes. The experimental conditions such as pressure, mass flow and heat fluxes are designed to replicate conditions similar to those in the micro-rocket cooling passages. In this chapter, the principles of the heat transfer experiment are explained, and a detailed description of the apparatus is presented. For the remaining part of the chapter, the data reduction procedure is developed and the uncertainty of the experiment is briefly addressed.

3.1 Principles of the Experiment [8,12,19]

During a test, hydrogen peroxide is flowed through a horizontal stainless steel test section. The test section is about 95.5 μm inside diameter, 305 μm outside diameter and is 4 mm in length. Two electrical connections are made across the test section as shown in Figure 3-1. The assembly is linked to a DC power supply and the test section is heated by virtue of its own electrical resistance. The heat dissipated within the microtube cross-section is absorbed by the flowing hydrogen peroxide through forced convective heat transfer. During a test, the mass flow is set constant and the power supplied is increased until the test section fails. Throughout the test, an outside wall temperature is measured using 2 different instruments: a thermocouple located at the test section exit and an infrared temperature sensor on a horizontally-moving carriage (see Figure 3-1).

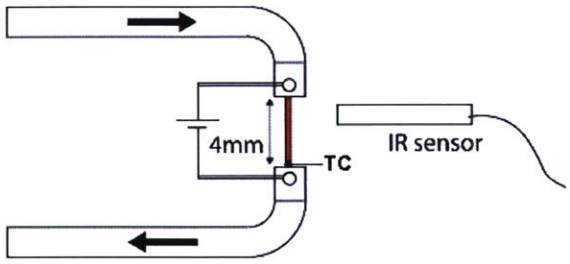

Figure 3-1: Schematic of the test section.

3.2 Experimental Apparatus

The experimental apparatus, originally designed by Loppata [19], was used in previous studies to investigate the cooling properties of supercritical ethanol [19], supercritical water [8] and JP7 [12], in stainless steel microtubes. For the current study, because of the handling and compatibility issues associated with hydrogen peroxide, most of the experimental apparatus was redesigned and rebuilt to ensure safer operation. Although the principle and instrumentation remain similar, the current experimental rig features a new fluid feed system, an added transfer and purge circuit, an improved control system and a video monitoring system. After a general overview of the rig, the following sub-sections describe in detail each component of the experimental apparatus, with a particular emphasis on the added features.

3.2.1 Overview

For safety reasons, the complete test rig has been divided between two rooms. The experimental apparatus is located in the micro-rocket engine test cell, whereas the computer, controls, power supplies and recording system are located in the control room [12]. The micro-rocket engine test cell is designed to conduct explosive experiments and consists of six 2 ft thick concrete walls closed by a ½" thick steel door. As will be explained in later sections, the rig can be operated from the control room and thus it is safe even in the case of a hydrogen peroxide explosion. An overview of the experimental apparatus and part of the control room are shown in Figure 3-2 and 3-3 respectively.

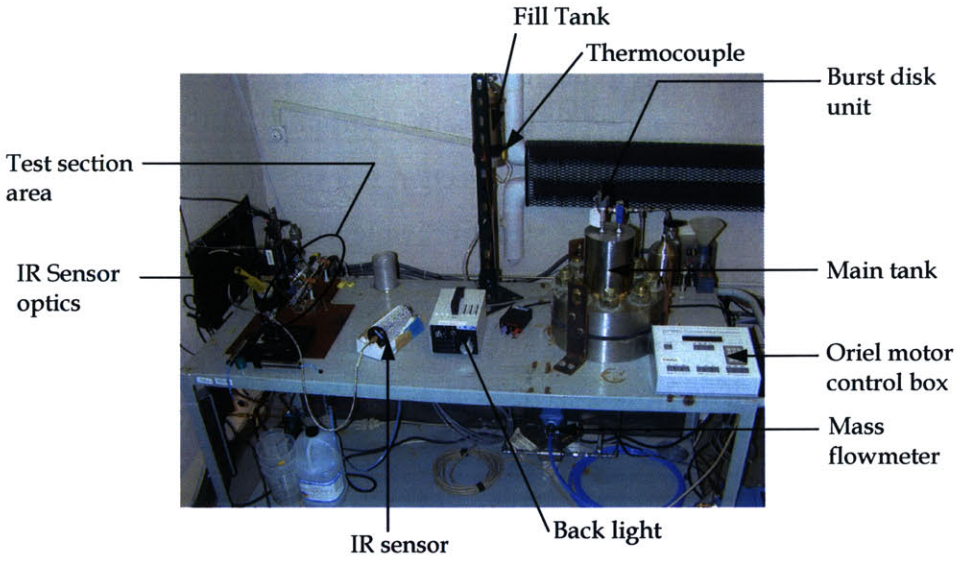

Figure 3-2: Front view of the experimental apparatus in the micro-rocket engine test cell.

Figure 3-3: Left view of the control room.

3.2.2 Test Section [12]

The test section is a U-shaped 304 stainless steel tube as shown in Figure 3-4. It has been fabricated by MicroGroup Inc [12] and consists of two 1/16" thick-walled tubes with 90° bends, in which a small microtube has been inserted. The microtube is 1 cm long and has an outer and inner diameter of 305 μm and 95.5 μm respectively. Of the microtube's

length, 3 mm are inserted into each of the 2 larger tubes leaving a nominal exposed length of 4 mm, as seen on Figure 3-4 [19]. The microtube is silver soldered in place and a black delrin cross piece is added for mechanical support [12,19]. The overall assembly is 1 1/8" wide, and 3" in length. The test section is installed on the test rig using 1/16" tubing Swagelok connections. The structural integrity of the test section has been confirmed by Joppin [12] for pressures up to 3,000 psi and temperatures up to 600°C. However, in the present series of tests, hydrogen peroxide explosions have been found to be sufficient to fail all of the test sections at the microtube.

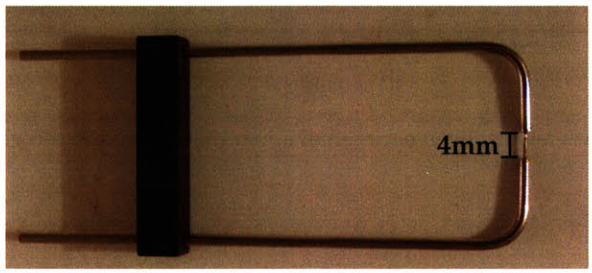

Figure 3-4: Test section picture.

3.2.3 Hydrogen Peroxide Feed System

The feed system consists mainly of pipes, valves and tanks, and its purpose is to feed hydrogen peroxide to the test section with the correct mass flow and pressure. A detailed schematic of the helium-fed hydrogen peroxide is presented in Figure 3-5, and some of the main components are labeled in Figure 3-6 and Figure 3-7.

3.2.3.1 Helium Circuit

The helium circuit is represented in blue in Figure 3-5. For this rig, helium is used as an inert pressurizing and feeding gas for the hydrogen peroxide and water circuits. It is supplied in large 6,000 psi bottles by BOC gases and is filtered downstream of the regulators using 316 stainless steel Swagelok filters. Although grade 4.5 helium is used, 0.5 µm filters are included to reduce risk of hydrogen peroxide contamination by foreign particles. To prevent backflow of peroxide into helium lines, Swagelok spring-loaded check valves are used on all feed lines. To further reduce the risk of backflow, a cracking

pressure of 25 psi was selected for the 6,000 psi-rated check valves. As an additional safety measure, burst disk units manufactured by Fike were installed on the main tank and dump tank helium feed. The complete unit consists of a 316 stainless steel 10,000 psi holding piece in which a calibrated 316 stainless steel rupture disk has been inserted. In case of a violent self-pressurizing reaction, the rupture disk would break at 5,000 psi and open a ½" port, thus preventing a catastrophic tank failure.

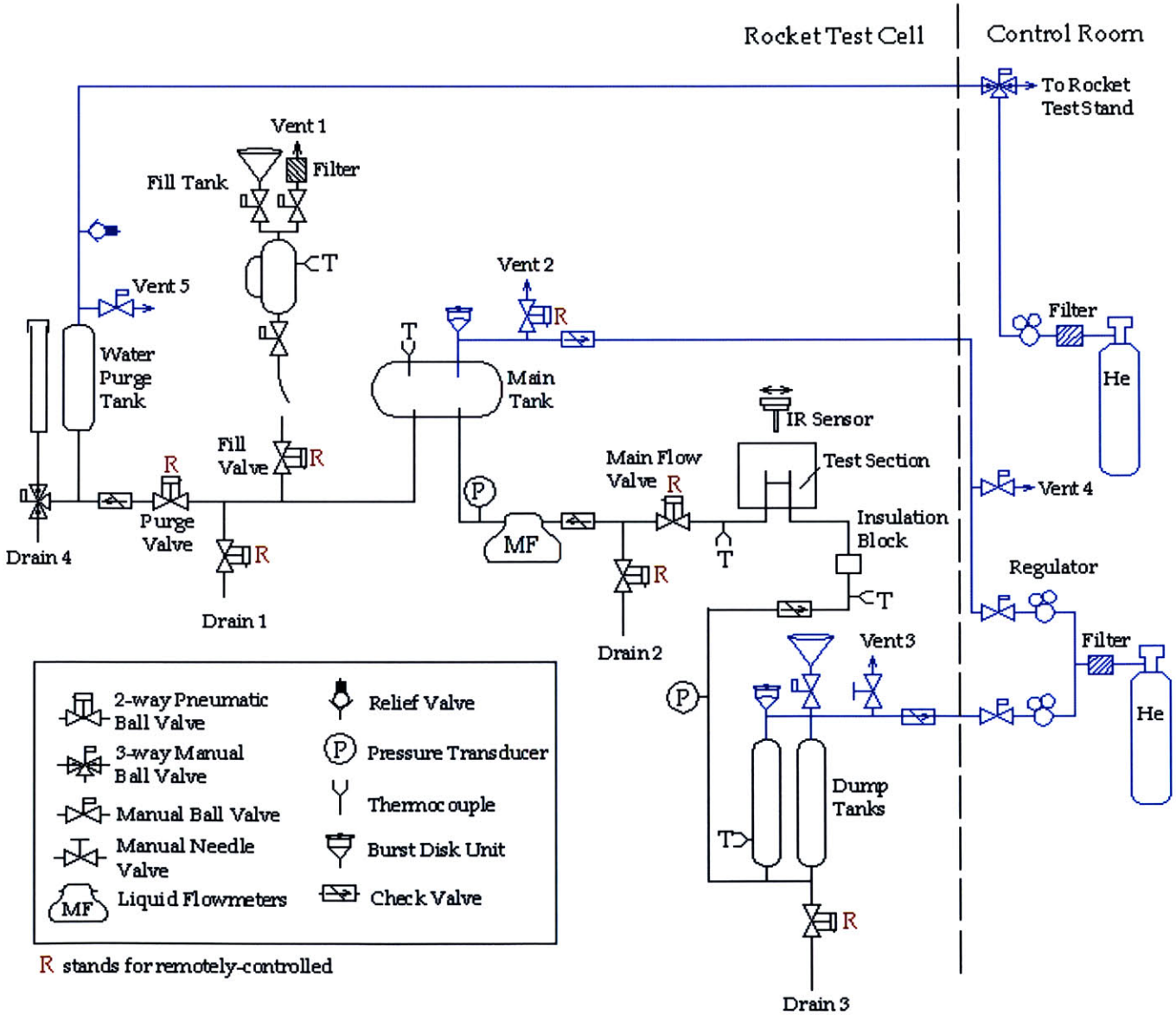

Figure 3-5: Schematic of the experimental apparatus.

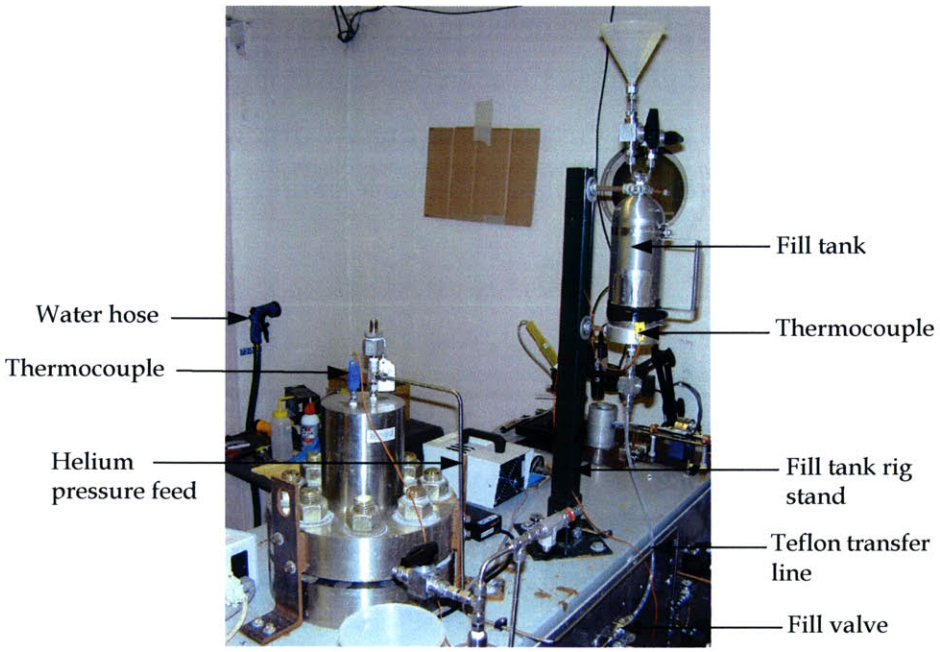

Figure 3-6: View of the hydrogen peroxide transfer system.

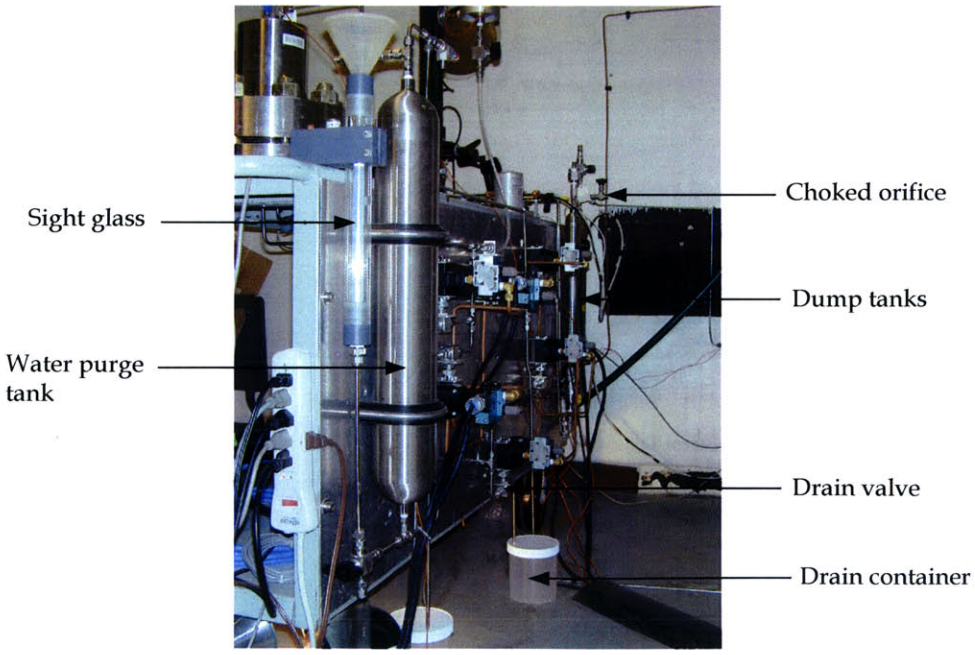

Figure 3-7: Backside view of the rig table (valve panel).

3.2.3.2 Hydrogen Peroxide Circuit

During a test, hydrogen peroxide flows from the main tank to the dump tank while passing through the test section. The main tank, made of 304 stainless steel, consists of a thick-walled 900 mL tank hydraulically tested to 7,500 psi [12,19]. The head of the tank and the flange are bolted together by eight 1.5" diameter bolts and are sealed by a Teflon® coated 321 stainless steel o-ring. As labeled in Figure 3-6, a K-type thermocouple is inserted into the main tank and is pressure-sealed using a Swagelok connection [19]. Immediately downstream of the main tank, the fluid flows through a pressure transducer and a coriolis-type mass flowmeter on its way to the test section [17]. All the piping on this section and on the rest of the test rig is done with ¼" thick-wall 316 stainless steel pipes and is rated to 7,500 psi. Downstream of the test section, the hydrogen peroxide flows through an electrically insulating block, which is there to prevent the current in the test section from shorting to ground [19]. This block is a Teflon® disk sandwiched between two 316 stainless steel pieces. The unit is constrained with 3/8" screws and nylon washers, thus electrically insulating the pipes located downstream. After the insulation block, the peroxide flows through a pressure transducer and is collected at the bottom of the dump tanks. During a test, the dump tanks are pressure-regulated using helium and a choked orifice, as labeled in Figure 3-7 [12]. The 6,000 psi pressure-rated dump tanks consist of two 316 stainless steel Swagelok tanks that sum to a volume of 1000 mL.

3.2.3.3 Hydrogen Peroxide Transfer and Purge Circuit

The remaining piping on the rig constitutes the hydrogen peroxide transfer and purge circuit. The purpose of the transfer system is to bring the hydrogen peroxide from the FMC supplied glass bottle to the main tank in a safe, controlled manner. A view of the transfer system is shown in Figure 3-6. The main component of this system is the fill tank, which is a 1000 mL 316 stainless steel Swagelok tank to which a flexible Teflon® line has been added as well as a polypropylene funnel. Prior to a test, the fill tank is evacuated and filled through the funnel under a clean fume hood. Then, the fill tank is brought back to the rig and the Teflon® line is attached to the rig. This allows the rig

operator to initiate the gravity-induced filling of the main tank from the control room. More details on this procedure can be found in section 3.2.8 and Appendix B.

The purpose of the purge circuit is to drain the hydrogen peroxide and to flush the pipe with water after a test. A view of the main components of this system is shown in Figure 3-7. The purge system is essentially a pressure-fed deionized water tank which is located upstream of the transfer system. It consists of a one gallon 316 stainless steel Swagelok tank that is helium-pressurized on top and connected to the peroxide circuit at the bottom. A Swagelok spring-loaded check valve is used at the bottom to prevent reverse flow into the tank. After the pipes have been purged with water, the rig is emptied through the three drains. A drain consists of a remotely controlled valve, a vertical steel tube and a water pre-filled polypropylene container. To reduce hydrogen peroxide splashing, the vertical ¼" pipes are fitted through a small hole in the container's cover. The water-filled 1200mL semi-transparent polypropylene containers have two purposes: to collect the 98% hydrogen peroxide and to instantaneously dilute it to a safer handling concentration (around 50%).

3.2.4 Heating System [19]

The microtube is electrically heated via two copper leads attached to the 1/16" outer diameter tubes adjacent to the test section [19], as shown in Figure 3-8. Each lead consist of two copper blocks in which a v-notch was machined, and the whole unit is attached with a small stainless steel cap screw. The electrical connections from the power supply to the leads are done through 10 gage copper wires brazed into brass bolts and inserted into the copper blocks [19]. Prior to that insertion, the wire's insulation was stripped and replaced with Teflon® tubing for hydrogen peroxide compatibility. To account for potential line losses, the voltage drop across the test section is obtained with a separate set of sense leads attached to the steel cap screws [12]. The power to the test section is provided by a 6260B Hewlett-Packard 1000 W constant voltage DC power supply. Given the small electrical resistance of the test section (~40 mΩ) this power supply was selected to provide low voltage (0-10 Volts) and high current (0-100 Amps) [19]. As mentioned in

the previous section, a non-conducting isolation block is included in the flow path downstream of the test section to isolate the non-grounded part of the tube (left side of Figure 3-8).

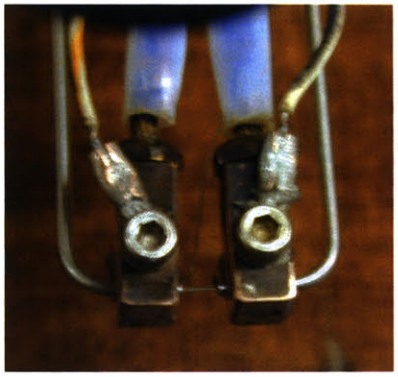

Figure 3-8: Test section electrical connection.

As a consequence of the above arrangement, the voltage drop measured at the cap screws includes not only the microtube's resistance but also the contact resistance between the copper leads and the steel. To minimize this unwanted contact resistance, conducting silver-based thread sealant (Goop®) manufactured by Crawford Fitting Company is applied at the interface between the tube and the copper leads. In addition, a 4-wire resistance measurement of the whole assembly is done prior to each experiment to verify the status of the connections. The silver-based thread sealant has been found to significantly reduce the assembly's resistance, from 70 mΩ originally to about 47 mΩ at room temperature. Although the assembly's resistance is not fully reduced to the test section's resistance (40 mΩ), a correction is developed in section 3.4.4 and the 4-wire measurement has been found to be useful in improving repeatability.

3.2.5 Measurements and Instrumentation

3.2.5.1 Pressure Measurement

The main tank and dump tank pressures are measured using an Omega PX603-5KG5V thin film pressure transducer. This transducer has an operating range of 0-5000 psi and has a factory quoted accuracy of ±20 psi. Despite being a class 3 material (Table 2-4), the

17-4PH stainless steel wetted parts have shown no compatibility problems with hydrogen peroxide.

3.2.5.2 Flow Measurement

The hydrogen peroxide mass flow is measured with a factory calibrated CFM010P MicroMotion Elite sensor. Its advertised zero stability and nominal flow range is 0.0011 g/s and 0-23 g/s respectively [19]. For the current experiment, the measured mass flow rate ranged from 0.2 to 0.8 g/s. By combining the effect of repeatability, linearity and hysteresis, the calibration accuracy of the flow meter for the range of flow measured is evaluated as ±0.007 g/s (see Appendix A). The flow meter wetted parts have shown no compatibility problems with hydrogen peroxide.

3.2.5.3 Power Measurement

The power delivered to the test section is obtained from the product of a current and voltage measurement. The current is measured using a 0-150 Amps shunt of known resistance, inserted into the 10 gage wire line out of the power supply [19]. For the voltage, the two cap screw leads of Figure 3-8 are directly linked into a high impedance data acquisition module.

3.2.5.4 Temperature Measurement

The fluid temperature in the main tank is measured with a T-type Omega thermocouple immersed in the fluid [12,19] as was pointed out in Figure 3-6. The temperature rise between the main tank and the test section assembly being negligible[6], this temperature measurement is taken as the fluid entrance bulk temperature.

The microtube outside wall temperature is measured using two different instruments, as underlined in Figure 3-9. First, an OS 1562 Omega infrared sensor originally used by Joppin [12] is used to measure the tube outside wall temperature axial profile. The full

[6] Here the test section assembly refers to the entire test section unit. Consequently, the temperature rise between the main tank and the test section assembly is negligible. See section 3.4.5 for details.

assembly consists of a power supply, a backlight, a cylindrical sensor and a set of lenses on a computer-controlled carriage. The components of this fast response fiber optic infrared sensor are shown in Figures 3-2 and 3-9. A measurement is obtained by pointing the lens assembly at the tube through a ¼" hole in an aluminum container, which has been added to prevent hydrogen peroxide spills. The carriage then moves horizontally along the tube and the computer records the position and temperature. As per the manufacturer's specs, this infrared sensor has a spot size of 0.01", a target length of 3" and a 5 ms response time. Its linear temperature range is set at 400-1,000°C with an output gain of 1 mV/°C and a calibrated accuracy of ±5°C.

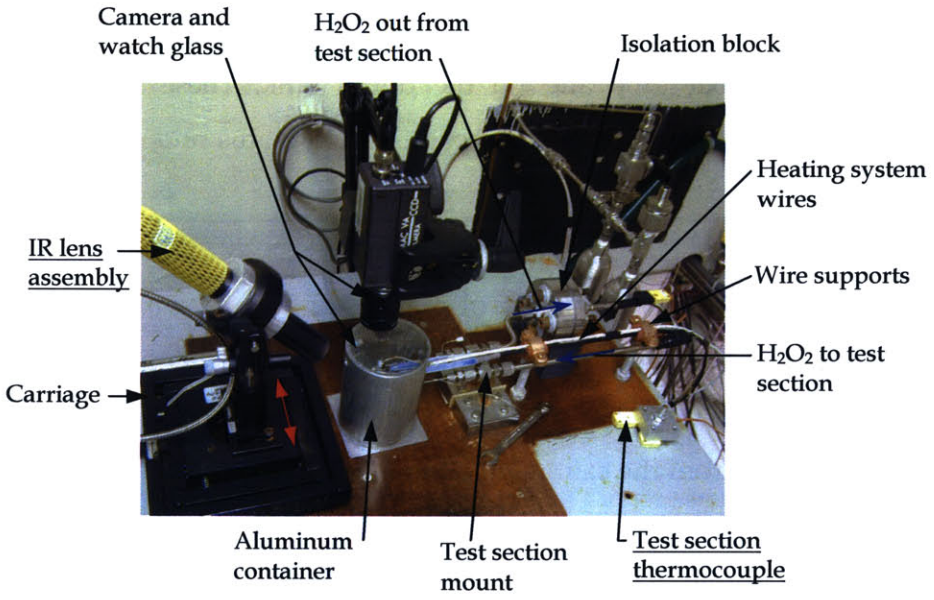

Figure 3-9: View of the installed test section.

Although microtube temperature profiles have been obtained for JP7 and JP10 by Joppin [12], no such data has been recorded with hydrogen peroxide given the limitations of the decomposition reaction. As will be shown in the next chapter, the decomposition reaction yielded an outside wall temperature too low over most of the tube's surface to be captured by the infrared sensor. Consequently, axial temperature profiles were not obtained, and the infrared sensor's position was held stationary at the microtube exit. This provided a measure of the microtube outside wall temperature at the exit, which is

known to be the hottest point on the tube, as confirmed by the observed microtube failure at that location for all tests.

Given the limitations of the infrared sensor, a K-type Omega thermocouple is used in addition to the sensor to measure the microtube's outside wall temperature at the exit plane. It is installed through one of the aluminum container's openings and is bonded on the tube surface using non-conductive ceramic paste. This instrument essentially replaces the infrared sensor for outside wall temperatures ranging from 150 to 350°C.

Finally, for safety purposes, temperature measurements using K-type Omega thermocouples are made on the outside of the fill tank, on the microtube entrance pipe, on the microtube exit pipe and on the dump tank. These measurements provide feedback to the rig operator on the decomposition status and serve as a safety check before entering the test cell (see Appendix B).

3.2.6 Data Acquisition and Control

The experiment control and data acquisition is done through a Dell Optiplex Pentium II PC running the software LabView [17]. The data acquisition system records the voltage and current signals from the calibrated shunt, voltage sense leads, pressure transducers, mass flowmeter, infrared sensor and thermocouples. The raw signal is sent through an Analog Devices signal conditioning and amplifier module of the 5B series and is converted to a 0-5 V signal, which is then handled by a National Instruments A/D board, model AT-MIO-64E-3 [17]. The data is displayed on the computer screen at a sampling rate of 4 Hz and saved to a text file at the end of the experiment. Figure 3-10 shows a screen shot of the LabView data acquisition and control interface.

To control the fluid flow paths, a subprogram has been written in LabView and its screen interface is shown in the top right corner of Figure 3-10. The controls are done via a digital I/O board, model PC-DIO-24PNP, which is used to control a set of solenoid valves, which in turn supply shop air to the pneumatic valve actuators [17]. The

solenoid valve, pneumatic actuator and the on/off ball valve are available pre-packaged from Swagelok under valve number SS-83KS4-31CD. With this installation, clicking on the red switches, depicted on the schematic, actuates the ball valves and allows risky operations such as filling and draining to be done remotely.

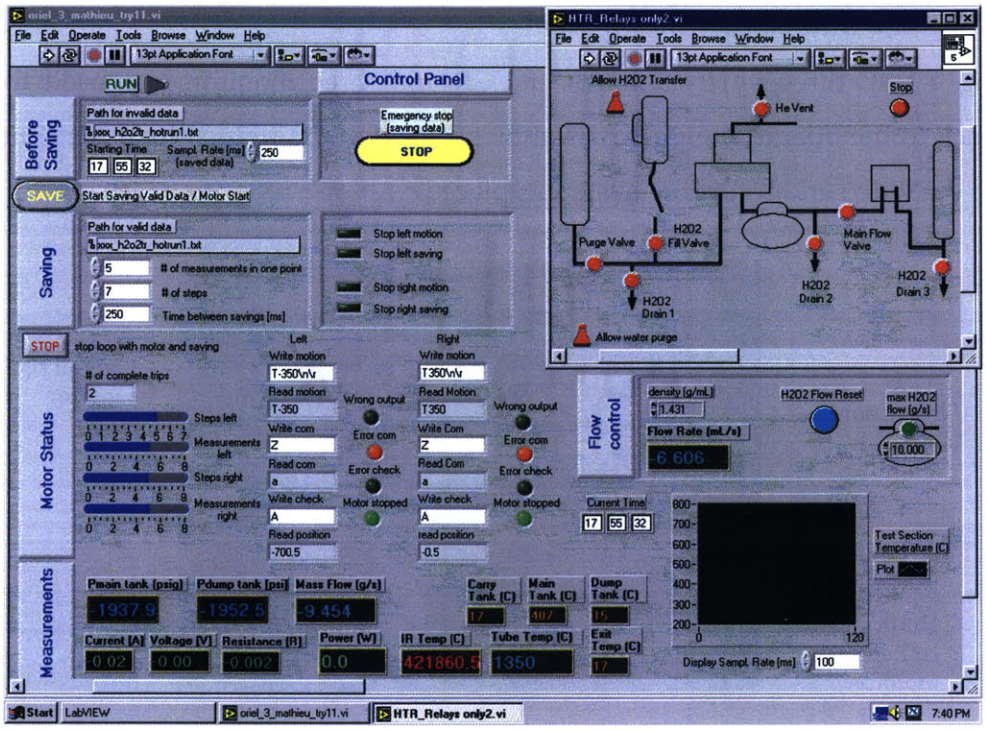

Figure 3-10: Screen shot of the LabView interface.

The fluid pressure and mass flow rate are controlled via three manual helium pressure regulators as follows. The pressure drop across the microtube determines the hydrogen peroxide mass flow rate, and the pressure level in the main and dump tanks determines the fluid's average pressure in the microtube [12,19]. In addition to the pressure regulation, the mass flow is controlled via an automatic shut-off valve that has been added for safety reasons. In case of a test section failure, the LabView control program includes a logic gate that detects the increase in mass flow and automatically shuts the main flow valve. This feature was found to be very effective in reducing extensive hydrogen peroxide spills.

The LabView interface is also used to control the infrared sensor, as shown on the mid right part of Figure 3-10. Because hydrogen peroxide tests did not allow extensive use of his control feature, the author refers interested readers to Joppin's work [12] for more details.

3.2.7 Video and Recording System

During a test, three video cameras, a VCR and three monitors are used to provide feedback to the operator. Figure 3-11 shows a view of the right side of the control room where the video and recording system is placed.

Figure 3-11: View of the right side of the control room.

The first camera is set to overlook the entire rig table and becomes particularly useful in case of a hydrogen peroxide spill (top right monitor). The second camera looks at the polypropylene containers and provides feedback during draining operations (bottom left monitor). Finally, as labeled in Figure 3-9, the third camera is set to look directly down at the test section through the aluminum container's watch glass. During a test, this view is particularly important because it is used to used to detect hot spots, to ensure mechanical integrity of the test section, to identify violent hydrogen peroxide reaction with the copper probes and to identify spills. Because this view is so critical, the video signal is recorded with a VCR and carefully reviewed after each experiment.

3.2.8 Experimental Procedure

The main experimental steps are briefly presented in this section. The exact checklists used during a test can be found in Appendix B.

Test Cell Preparation

1. Prepare fill tank: The fill tank is rinsed with water, evacuated and brought to the fume hood where it is ready for filling.
2. Prepare purge system and drains: The purge tank deionized water level is checked, the drain camera is focused and a bypass test section is installed on the rig.
3. Purge residual hydrogen peroxide: The diluted hydrogen peroxide from previous runs is purged out of the rig with helium.
4. Dump tank water filling: Because of the potential for hot hydrogen peroxide coming from the test section to initiate a strong decomposition reaction, the dump tanks are evacuated and filled half way (500 mL) with water. This ensures at most a concentration of 50%.
5. Install test section: At this step, the microtube test section replaces the bypass installed previously. The copper probes are carefully attached on the adjacent tubes and silver goop is applied at the interface. A 4-wire resistance measurement is made to ensure good electrical contact. The test section thermocouple is bonded on the microtube using ceramic paste.
6. Set aluminum container: The protective aluminum container is filled half way with water and is slid on the test section. The test section camera is set over the watch glass and focused.
7. IR alignment: The infrared sensor carriage is aligned with the microtube using the backlight. A few scans are made before the sensor is considered aligned.
8. Getting dressed: At this point the operator dresses with a full body PVC suit, Neoprene gloves and boots, safety goggles and a full face shield. This suit is worn until the very last step when the hydrogen peroxide is disposed.
9. Bring hydrogen peroxide to test cell: This step typically involves transferring 500

mL of hydrogen peroxide from its original FMC glass bottle into the fill tank. It is carefully done under a clean fume hood. Then, the fill tank is brought to the test cell and attached on its stand. The test cell door is closed and from this point on, the operation of the rig is done remotely.

Test Procedure

1. Main tank filling: The hydrogen peroxide in the fill tank is transferred by gravity to the main tank.
2. Start mass flow: The main tank and dump tank pressures are selected and the main flow valve is open. The hydrogen peroxide mass flow settles and is adjusted to the desired value.
3. Ramp power: The test section power supply is enabled and the current is ramped in small increments until the test section fails. During this process, the microtube's mechanical integrity is assessed with the monitor and its temperature is obtained with the infrared sensor and the thermocouple.
4. Rapid shutdown: For a test section failure, the power supplied and the hydrogen peroxide mass flow are automatically shut off. The main tank and dump tank are remotely vented and the dump tank temperature is carefully assessed. For a case where its temperature is judged too high (>50°C), the dump tanks are sprayed with water using a water hose in the test cell.

Purge and System Shutdown

1. Drain hydrogen peroxide: Using the drain camera as feedback, every valve is cycled and the hydrogen peroxide is drained into the polypropylene containers.
2. Initial water purge: Deionized water from the purge tank is flowed through every part of the rig and is drained in the polypropylene containers.
3. Return to test cell: At this point, the test cell is judged safe to return and the floor is flooded with water upon entry. The polypropylene containers are emptied, the test section area is sprayed with water and the microtube is replaced with the bypass.

4. Final water purge: The water purge step is repeated and critical areas of the rig are filled with water until the next series of tests.
5. Dispose of hydrogen peroxide: The high concentration peroxide (~50%) collected from the polypropylene containers is diluted to a concentration of about 2% at which point it is disposed.

3.3 System Calibration

This section discusses the experimental calibration of the pressure transducers and of the infrared temperature sensor [7]. It also describes the various methods used in determining the test section geometry and establishes its resulting dimensions.

3.3.1 Pressure Transducers

The reference pressure for the calibration of the pressure transducers was obtained using a 6000 psi Heize gauge, which has a stated full scale accuracy of 0.25%. Helium was used as the pressurizing gas and the pressure was increased in increments of about 500 psi for the entire operating range (0-4000 psi). For each pressure setting, the transducer's output voltage was obtained from LabView and was compared with the reference pressure. This calibration process was repeated every four months and the slope of the linear fit was found to vary by less than 1%. A typical calibration curve for both pressure transducers is shown in Figure 3-12.

3.3.2 Infrared Temperature Sensor

The infrared temperature sensor was shipped pre-calibrated by the manufacturer. As stated in the manual, the calibration was done using a reference black body surface and yielded a linear output gain of 1 mV/°C for a temperature range of 400-1,000°C. However, in order to use this calibration, the targeted surface has to be flat and its emissivity has to be known. In the present case, where a 304 stainless steel tube is used, the surface targeted is not flat. Furthermore, as it is the case with other metal, the

[7] The mass flow meter was pre-calibrated at the factory.

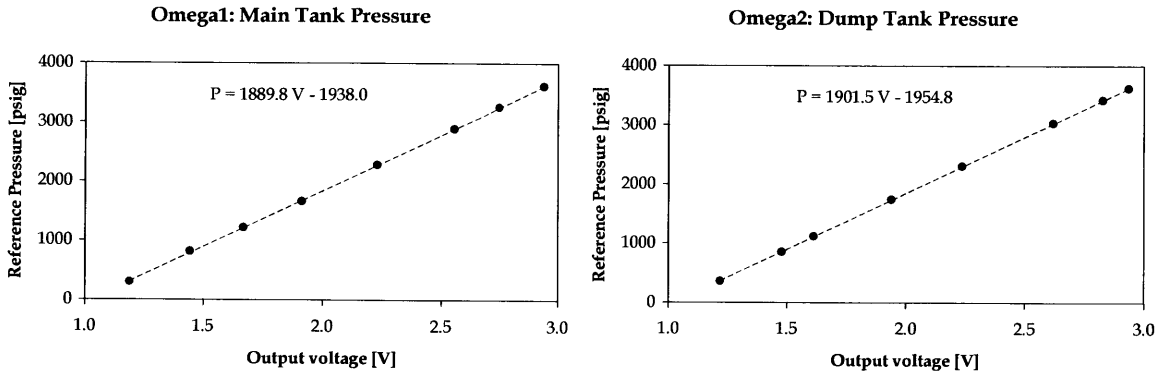

Figure 3-12: Pressure transducer calibration.

condition of the surface has a big impact on the emissivity. For example, for 304 stainless steel, the emissivity can vary from 0.07 for a polished surface, to 0.70 for a surface subjected to repeated heating [15].

To avoid the problems described above, an in-house calibration was performed using a thermocouple as the reference temperature. In this procedure, developed by Joppin [12], the infrared sensor is aimed at the weld of a stainless steel thermocouple. The thermocouple is then heated using a propane flame up to 1,800°C. During cool down, the voltage output from the sensor and the thermocouple temperature were sampled at a rate of 100Hz. The resulting calibration curve is shown in Figure 3-13. Note that a linear slope was obtained for temperatures above 450°C with deviations of about ±15°C. As shown in Figure 3-13, the calibration curve was extended below the linear range down to a temperature of 350°C, the minimum allowed by the sensor. This portion of the curve, accurate only to ±25°C, was derived in hope of reading the low temperature profiles allowed by hydrogen peroxide. As mentioned in section 3.2.5.4, no profile has been obtained and this instrument has only been used in conjunction with a thermocouple at the microtube's exit plane. For high mass flow cases (>0.6 g/s), the hottest temperature point on the outside wall of the microtube was greater than 350°C and thus a stationary infrared sensor measurement was obtained.

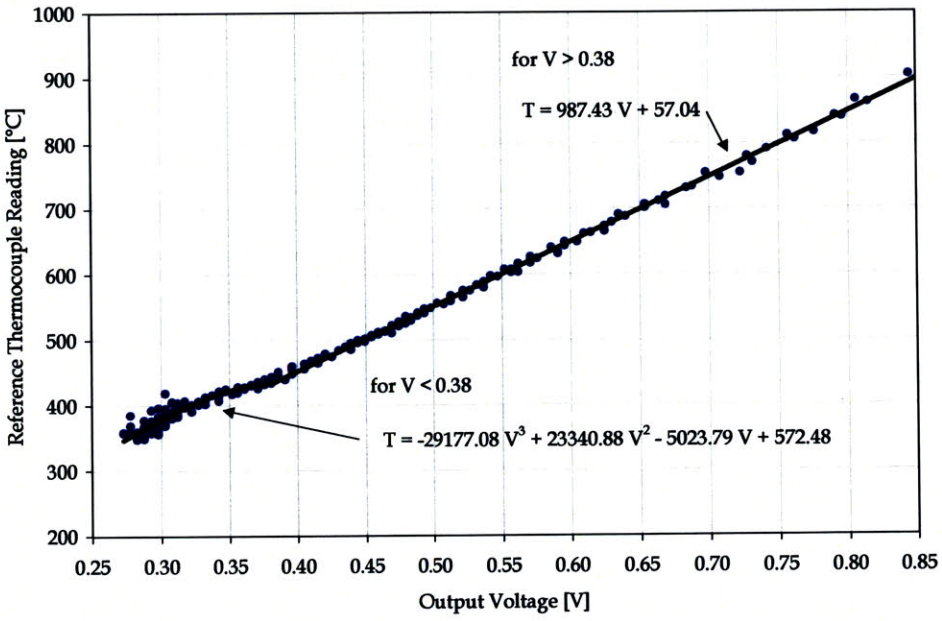

Figure 3-13: Infrared temperature sensor calibration.

3.3.3 Test Section Geometry

The issue of determining accurately the test section geometry naturally arises from the small dimensions involved and the manufacturing tolerances available. Because of its importance in the data reduction, this section establishes the test section dimensions to be used in future calculations.

Given the importance of the microtube geometry for the data reduction, water[8] flow versus pressure data was obtained for each microtube. It was then compared with a standard pressure drop model developed using the Moody chart as well as entrance and exit losses [23]. An example of this comparison for test section number 315 is shown in Figure 3-14. In this representative test, the flow data suggests a microtube inside diameter of 95.5 μm with an uncertainty of ±1.5 μm. By comparing the flow data for all microtubes, the mean inside diameter was found to be 95.5 μm with a variation between tubes of at most 0.5 μm. To further confirm this dimension, the microtube inside

[8] Although this could have been done with hydrogen peroxide, water was preferred because of its well-known physical properties at all temperatures.

diameter has previously been recognized as an important parameter by Lopata [19] and his estimation, based on flow data, pressure correlations and computational fluid dynamics also yielded a value of 95 μm for the inside diameter.

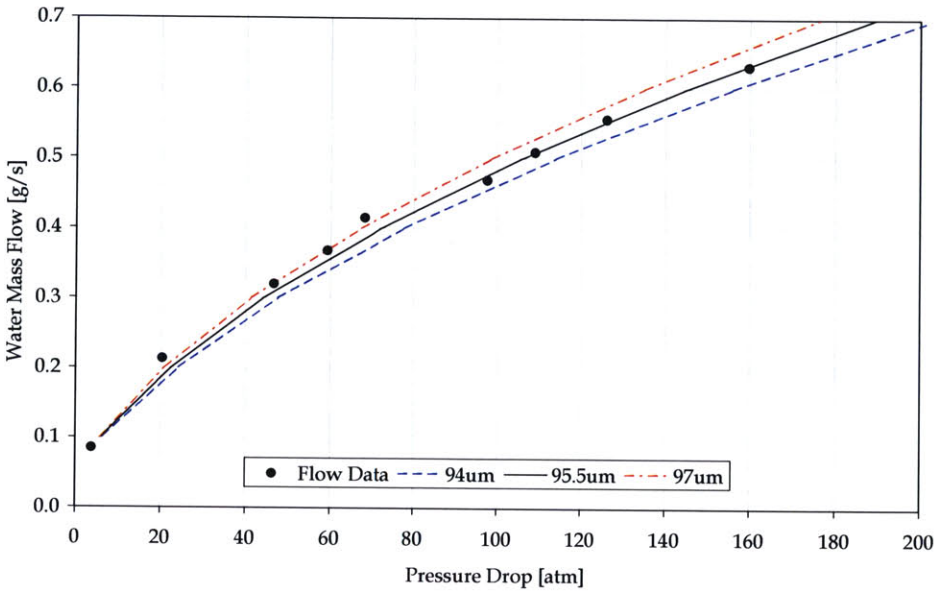

Figure 3-14: Microtube 315 inside diameter sizing through water flow test.

To estimate other geometrical features of the test section, a microtube was encapsulated in epoxy and polished perpendicular to its length to reveal its cross section. Then SEM pictures were taken at different cross sections along the length of the tube. The measurements taken from the picture revealed on average, a 1/16" tube inside diameter of 394 μm, a microtube outside diameter of 305 μm and confirmed the 95.5 μm microtube inside diameter obtained from the flow data. Due to the variation in geometry along the length of the test section, the uncertainty on the above SEM measurements has been estimated to ±4 μm and ±15 μm respectively.

The last test section geometrical feature of interest is what is referred to in this thesis as the microtube resistive length. This length, which is the distance between the two silver solder joints at either end, is responsible for the resistive heat dissipation, most of which is absorbed by the hydrogen peroxide. Nominally, the resistive length should be 4 mm,

but it is not, because of the conical shape of the silver solder. An estimation for the resistive length was first made at 3.65 mm using a 0.02 mm accurate Vernier caliper in combination with a microscope. This value was later confirmed through a comparison between a theoretical microtube electrical resistance and a direct measurement. The theoretical resistance R_{THEORY} is estimated from the conductive properties of 304 stainless steel as follows [24]:

$$R_{THEORY} = \frac{4\rho L_{res}}{\pi(d_o^{\,2} - d_i^{\,2})} \tag{3.1}$$

where R_{THEORY} is the theoretical microtube resistance in Ohms, d_o is the microtube outside diameter in m, d_i is the microtube inside diameter in m, and ρ, the resistivity of 304 stainless steel, is 731.7×10^{-9} Ω-m at 20°C [24].

From the above expression the theoretical resistance of the microtube is estimated at 40.5 mΩ, at room temperature. This is consistent with the value of 40 mΩ mentioned in section 3.2.4, and thus confirms the resistive length measured with the microscope.

A summary of the test section geometrical parameters determined in this section is presented in Table 3-1.

Symbol	Description	Dimension	Uncertainty
d_i	Microtube inside diameter	95.5 µm	±2.0 um
d_o	Microtube outside diameter	305 µm	±4 um
L	Microtube length	1.03 cm	-
L_{res}	Resistive length	3.65 mm	±0.05 mm
D_i	1/16" tube inside diameter	394 µm	±15 um
D_o	1/16" tube outside diameter	1600 µm	-

Table 3-1: Test section important parameters.

3.4 General Data Reduction [8,12]

3.4.1 Measured Parameters

For each experiment, we obtain time samples of the following set of data: inlet and outlet pressures, mass flow, temperature of the fluid in the main tank, current and voltage supplied to the test section as well as the outside wall temperature at the exit of the test section [12]. On rare occasions, a temperature scan was obtained along the tube. In such cases, the additional data consist of an outside wall temperature measurement, its position along the tube and its evolution in time.

From these measurements, we can derive the power supplied to the test section assembly, the hot electrical resistance of the assembly, the power dissipated by resistive heating of the small test section, the inside wall temperature, the bulk temperature and an estimate the heat transfer coefficient. In almost all cases, these calculations have been performed with experimental data corresponding to the test section failure point

3.4.2 Power Supplied

The power Q supplied to the test section assembly (including the copper blocks and the larger size stainless steel tube) is simply the product of the current I flowing through the assembly and the voltage V measured at the copper leads [8,12].

$$Q = I V \tag{3.2}$$

where Q is the power in Watts, I is the current in Amps and V is the voltage in Volts.

3.4.3 Electrical Resistance of the Assembly

The electrical resistance of the test section assembly R_{TOT} constitutes the sum of the stainless steel microtube resistance, with the contact resistance between the copper leads and the 1/16" tube. It is calculated from a measurement of the current I flowing through the assembly and the voltage V measured at the copper leads.

$$R_{TOT} = \frac{V}{I} \tag{3.3}$$

where R_{TOT} is the resistance in Ohms, I is the current in Amps and V is the voltage in Volts.

3.4.4 Power Dissipated

The power dissipated by resistive heating of the microtube Q_{DISS} is a fraction of the total power supplied to the test section Q. Its value depends on the relative importance of the microtube's resistance R_{TUBE} compared to the total resistance of the assembly R_{TOT}.

$$Q_{DISS} = \left[\frac{R_{TUBE}}{R_{TOT}}\right] Q \tag{3.4}$$

where Q_{DISS} and Q are the power quantities in Watts; R_{TUBE} and R_{TOT} are resistances in Ohms. The resistance of the microtube has been measured experimentally and was found to be 40 mΩ at room temperature. However this value is not used directly in the expression above. Due to the strong conductivity variation of 304 stainless steel with temperature [24], a correction is applied for each test and a resistance of about 44 to 47 mΩ is used instead, in the calculation. This correction accounts for a metal bulk temperature increase of approximately 115°C to 200°C.

3.4.5 Bulk Temperature

The mixing-cup, or bulk temperature $T_b(x)$ of a fluid at an axial position x along the tube is defined as the ratio of the rate of flow of enthalpy through a tube cross section, with the rate of flow of heat capacity through the same tube cross section. In other words, if the tube was allowed to discharge its fluid into a mixing cup at a distance x, the fluid temperature in that cup would be $T_b(x)$ [15].

Here the bulk temperature $T_b(x)$ is calculated using an energy balance between the entrance plane of the microtube and any arbitrary plane located a distance x downstream. In between those two planes, resistive heating of the microtube provides a uniform heat flux to the fluid. In doing this calculation, longitudinal conduction in the steel microtube and heat loss to the room through radiation are assumed to be negligible compared to forced convection inside the 95.5 μm tube (see section 3.5.3 for more details). Given this assumption, the power dissipated by resistive heating Q_{DISS} is fully absorbed by the fluid and the bulk temperature in the microtube can be expressed as follows [8,12]:

$$T_b(x) = T_b(0) + \frac{Q_{DISS}}{\dot{m} Cp}\left[\frac{x}{L_{res}}\right] \tag{3.5}$$

where $T_b(x)$ is the fluid bulk temperature at axial position x in °C, $T_b(0)$ is the bulk temperature at the entrance in °C, Q_{DISS} is the power dissipated in Watts, $\dot{m}$ is the mass flow in kg/s , Cp is the heat capacity in J/kg-K , x is the axial position in mm and L_{res} is the resistive length of the tube in mm. In this expression, Cp is considered constant and equal to 2650 J/kg-K and L_{res} is 3.65mm, as discussed previously in section 3.3.3 .

To evaluate $T_b(x)$ as given in equation 3.5, an estimation for $T_b(0)$, the bulk temperature at the entrance plane of the microtube, is needed. Previous studies have assumed this parameter to simply be the temperature of the fluid measured in the main tank [8,12,19]. However, this assumption is inadequate in the present study because it neglects a considerable portion of the heat dissipated at the copper-steel interface. Instead, a simple resistance analysis was carried out and showed that the large convective heat transfer coefficient in the 1/16" tube (~6×10^3 W/m^2-K) was sufficient to consider longitudinal conduction in the steel walls to be negligible compared to forced convection. Therefore, the fluid temperature is increased at the first copper lead connection, prior to its entry in the microtube. By assuming the total heat dissipated at the copper-steel interface to be

evenly split between the two leads, the fluid bulk temperature at the entrance plane of the microtube is estimated by:

$$T_b(0) = T_{TANK} + \frac{1}{\dot{m} Cp}\left[\frac{Q - Q_{DISS}}{2}\right] \tag{3.6}$$

where T_{TANK} is the fluid temperature in the main tank in °C, Q_{DISS} and Q are the power quantities in Watts, $\dot{m}$ is the mass flow in kg/s and Cp is the heat capacity in J/kg-K.

3.4.6 Inside Wall Temperature [8,12]

In this section, the inside wall temperature $T_i(x)$ is calculated from a radial energy balance and a measurement of the outside wall temperature $T_o(x)$. As mentioned before, the fluid temperature and thus the tube inside wall temperature rises due to the energy dissipation by the electric field along the 3.65 mm long stainless steel microtube. In this calculation, the electric field and therefore the current is assumed constant over the radius.

Consider an annular control volume of length dX, inner radius r and outer radius r_o as illustrated in Figure 3-15. At steady state, the heat generated inside the stainless steel annulus flows radially towards the inner wall of the tube since all other heat transfer paths are negligible (see section 3.5.3 for more details). At a radial position r, the energy flows inwards by conduction and is given by Fourier's Law:

$$q_{CONDUCTION} = q''_w A = k_{ss} \left.\frac{dT}{dr}\right|_r (2\pi r) dX \tag{3.7}$$

where $q_{CONDUCTION}$ is the power conducted through plane r, k_{ss} is the thermal conductivity of 304 stainless steel, r is the radial distance from the centerline of the tube, dX is an infinitesimal distance along the axis and T is the temperature as a function of r.

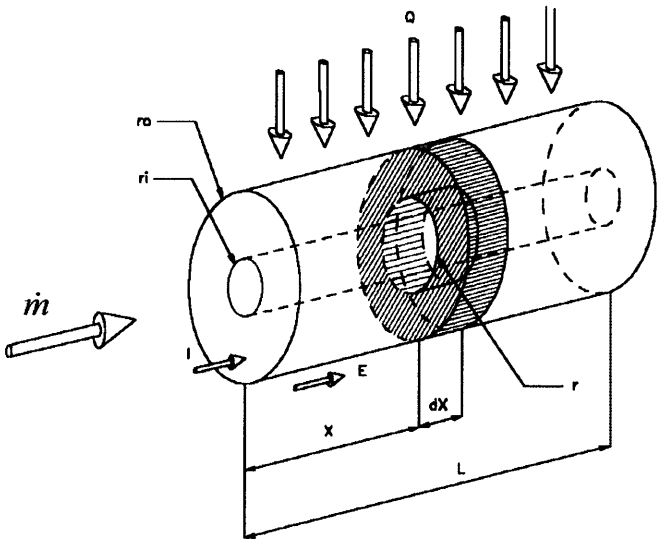

Figure 3-15: Radial conduction model for the microtube [12].

Moreover, the power dissipated by resistive heating in the annulus is given by:

$$q_{DISSIPATED} = \left[\int_{r}^{r_o} \sigma_{ss} E^2 (2\pi r) dr \right] dX \tag{3.8}$$

where $q_{DISSIPATED}$ is the power dissipated in the annulus, σ_{ss} is the electrical conductivity of 304 stainless steel, E is the electric field, r is the radial distance from the centerline of the tube and dX is an infinitesimal distance along the axis.

Since the power generated in the annulus is conducted inwards through the cylindrical shell of radius r, expressions 3.7 and 3.8 can be equated and simplified as follows:

$$r k_{ss} \left. \frac{dT}{dr} \right|_r = \int_{r}^{r_o} \sigma E^2 r dr \tag{3.9}$$

This equality is integrated on the right hand side and separation of variables becomes possible, given the variation of thermal conductivity with temperature. From a materials

handbook [24], the thermal conductivity of 304 stainless steel was found to obey the following linear profile:

$$k_{ss} = 0.0152T + 14.2444 \tag{3.10}$$

After an indefinite integration, an expression for temperature as a function of radius and electric field intensity is obtained:

$$0.0076T^2 + 14.2444T = \frac{\sigma E^2}{4}\left[r_o^{\,2} \ln r - \frac{r^2}{2}\right] + K \tag{3.11}$$

where K, the constant of integration, can be eliminated from the equation by making use of the following boundary conditions:

$$\begin{aligned} r &= r_o \,,\, T = T_o \\ r &= r_i \,,\, T = T_i \end{aligned} \tag{3.12}$$

The final expression can be further simplified by noting that the σE^2 term can be expressed as a function of the total power dissipated by resistive heating in the stainless steel microtube, Q_{DISS}:

$$\sigma E^2 = \frac{2\,Q_{DISS}}{L\pi(r_o^{\,2} - r_i^{\,2})} \tag{3.13}$$

After the substitutions, the inside wall temperature can finally be expressed as a function of the outside wall temperature measurement, the power dissipated by resistive heating and geometry [8,12].

$$T_i = -937.13 + 65.79\sqrt{202.90 - 0.0304B} \tag{3.14}$$

with

$$B = \frac{Q_{DISS}}{2\pi L_{res}}\left[\frac{\ln(r_i/r_o)}{1-(r_i/r_o)^2} + \frac{1}{2}\right] - 14.2444T_o - 0.0076T_o^{\,2} \tag{3.15}$$

where T_i is the inside wall temperature in °C, T_o is the outside wall temperature in °C, Q_{DISS} is the power dissipated by resistive heating in Watts, L_{res} is the resistive length of the microtube , r_o is the tube outside radius in m and r_i is the tube inside radius in m.

3.4.7 Heat Transfer Coefficient

The heat transfer coefficient h is associated with the forced convective heat transfer between the microtube wall and the fluid. Accordingly, it is obtained from the difference between the inside wall temperature and the bulk fluid temperature as follows [15]:

$$h = \frac{Q_{DISS}}{A_i(T_i - T_b)} \tag{3.16}$$

where Q_{DISS} is the power dissipated by resistive heating in Watts, A_i is the inside wall surface in m^2, and T_i and T_b are the inside wall and bulk temperatures in °C.

3.5 Experimental Issues and Uncertainty

In this section, experimental issues and uncertainty are identified to assess the validity of the results presented in this thesis [12]. First, the limitations inherent to the design of the experiment are addressed. Then, a distinction is made between the experimental uncertainty associated with physical modeling and the one associated with the apparatus uncertainty. Although the issue of experimental uncertainty and its propagation is briefly presented in this section, a detailed analysis can be found in Appendix A.

3.5.1 Experiment Limitations

The main experimental limitation on the conditions tested comes the infrared temperature sensor. Because of the hydrogen peroxide decomposition, the maximum temperature registered at the surface of the tube ranged between 260 and 350°C, depending on test conditions. The infrared sensor, which has a 350-1000°C temperature range, was found to be inadequate for most outside wall temperature measurement. Although a temperature measurement was still obtained with a thermocouple, it is an intrusive method and its measurement does not yield outside wall temperature profiles. This seriously limits the amount of data available from a test and increases the uncertainty of the results obtained. Clearly, an infrared sensor with a temperature range of 100-500°C would have been more adequate for the present study.

3.5.2 Experimental Uncertainty

Appendix A presents a detailed analysis of the uncertainty in the measured and derived quantities [17]. Table 3-2 shows an example of uncertainty analysis for a typical test result presented in chapter 4.

Parameter	Typical Value	Uncertainty	% Uncertainty
$\dot{m}$ [g/s]	0.632	± 0.007	± 1.1%
Q [W]	137.9	± 2.4	± 1.7%
T_o [°C]	345	± 12	± 3.5%
$T_b(out)$ [°C]	90.4	± 3.5	± 3.9%
T_i [°C]	146	± 17	± 12%
h [10^6 W/m^{2}K]	1.71	± 0.55	± 32%

Table 3-2: Example of uncertainty analysis.

3.5.3 Validity of the Physical Model

The main modeling assumption made in the data reduction is the one stating that all the heat generated by resistive heating is absorbed by the fluid. There are potentially heat

losses to the room through radiation and natural convection. In addition, longitudinal conduction in the stainless steel wall could be an issue and needs to be evaluated.

After analysis, all of the loss mechanisms mentionned above were found to be negligible. Upper bounds on radiation and natural convection losses were established at 0.03 W and 0.01 W respectively, assuming a large microtube outside wall temperature of 400°C. These losses are clearly negligible compared to the 50 W of heat dissipated in a typical experiment. Longitudinal conduction was also found to be negligible compared to the heat conducted radially in the fluid. Due to the large convective heat transfer coefficient achieved in the microtube (~10^6 W/m^2K), the longitudinal conduction losses in the stainless steel walls were evaluated at approximately 0.1% of the total heat transfer.

The remaining modeling assumptions to address are the ones related to the fluid temperature increase prior to its entry in the microtube. In a typical experiment, the microtube dissipation is responsible for about 75% of the total dissipation. The rest is dissipated at the two copper-steel interfaces. As mentioned in the data reduction, two assumptions are made to calculate the bulk fluid temperature at the entrance:

- the heat dissipated is assumed to be fully absorbed by the fluid.
- the dissipation is assumed to be evenly split between the two copper leads.

The first assumption was verified using a simple resistance analysis, which showed that longitudinal conduction in the steel walls is negligible compared to forced convection. In addition, a 1/16" tube outside wall measurement was taken during a test and showed no temperature increase near the copper leads. This confirms that the fluid absorbs nearly all the heat dissipated at the lead and validates the first assumption.

To verify the second assumption, a 4-wire resistance measurement of one half of the electrical assembly was made and showed a resistance split varying from the ideal case of 50%/50% to at most 44%/56%. This translates into an uncertainty of ±1°C in the

entrance temperature estimated. Since this is smaller than the thermocouple measurement uncertainty, it is considered negligible.

3.6 Summary

This chapter has described the principles of the heat transfer experiment, the experimental apparatus, the data reduction procedure and has reviewed key modeling assumptions. The next chapter will present and discuss the results obtained for the hydrogen peroxide heat transfer tests.

Chapter 4

Experimental Results and Discussion

The principles of the heat transfer experiment designed to test hydrogen peroxide in microtubes have been presented. In this chapter, after an overview of the type of tests performed, the results obtained from the 98% H_2O_2 heat transfer tests are presented and analyzed. As per the objective of this study, a stability limit associated with the thermal decomposition of HTP is defined and the heat transfer rates available from hydrogen peroxide cooling are characterized.

4.1 Testing Overview

All the heat transfer tests were conducted with the same procedure. First, the desired pressure level in the dump tank was set. Then, the inlet pressure was set depending on the desired hydrogen peroxide mass flow. After the flow stabilized, the power delivered to the test section was increased slowly until the hydrogen peroxide exploded and the tube failed. For the current study, all tubes have been tested to failure. The following sub-sections provide more details by summarizing, quantitatively, the experiments performed and by showing the evolution of the important parameters for a typical test.

4.1.1 Summary of the Performed Experiments

Heat transfer tests have been conducted with hydrogen peroxide at pressures, mass flows and length scales relevant for the design of the micro-rocket engine. A total of 13 tests have been performed using 98% hydrogen peroxide in 95.5 μm tubes with a mass flow ranging from 0.23 to 0.68 g/s for a corresponding Reynolds Number range of 4,800 to 14,000. The microtube exit pressure was varied from a low value of 37 atm to as high as 218 atm, which is slightly above the critical point of hydrogen peroxide at 214 atm. In order to obtain the necessary mass flows, pressure values at the inlet were varied between 81 and 294 atm. Initially, outside wall temperature measurements were only made with the infrared temperature sensor. However, due to the low temperatures allowed by hydrogen peroxide explosions, a thermocouple was added for the measurement, in later tests. Consequently, only the last 6 tests have outside wall measurements, which ranged from 230°C to 345°C. For the results presented, only the last 6 data points are available for the full analysis; the remaining 7 tests are used whenever possible.

4.1.2 Typical Test Evolution

During a test, the controlled parameters are the hydrogen peroxide mass flow via the pressure regulators, and the power to the test section assembly, via the power supply [12]. Figure 4-1 shows the time evolution of those controlled parameters for test section number 311. As can be seen from the figure, the mass flow is kept constant at 0.63 g/s until failure occurs at approximately 517 s. At that point, the mass flow goes up temporarily before the automatic shut-off valve suppresses the flow. Also shown in the figure is the power supplied to the assembly, which is initially increased to about 90 W, a known safe level for this particular test. After this rapid increase (using the coarse knob), the power supplied is increased at a much slower rate (using the fine knob) until the heat flux level, and correspondingly the hydrogen peroxide temperature, triggers an explosion. This happens at 138 W for this particular test.

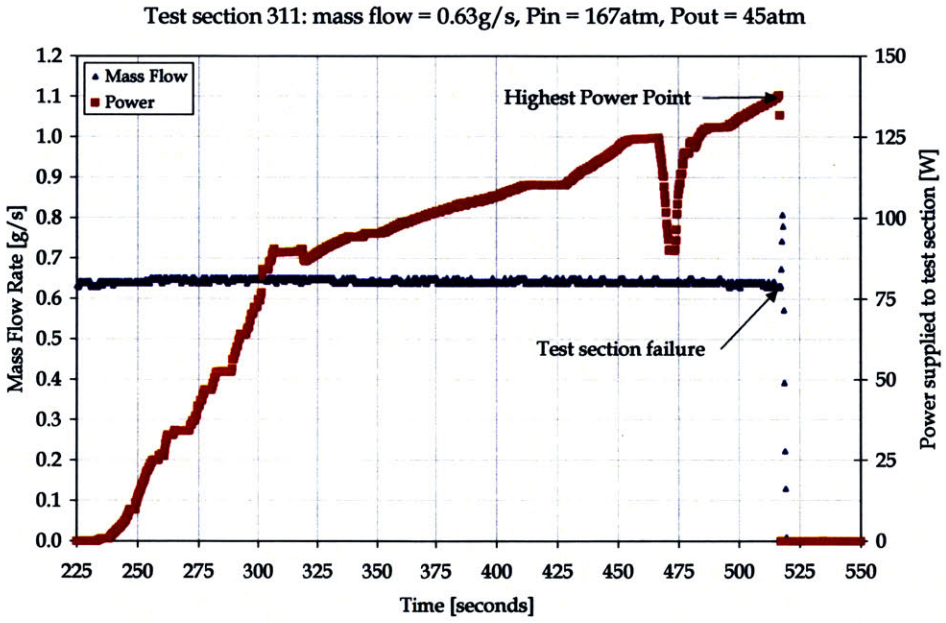

Figure 4-1: Typical evolution of the controlled parameters. Mass flow and power supplied vs. time for test section 311. Note that the sudden drop in power at 470sec is non-physical and is a consequence of the limited range of the fine knob on the power supply, which requires a corresponding power increase with the coarse knob.

Figure 4-2 shows the corresponding video frame sequence of the hydrogen peroxide explosion, for test section 311. This sequence is provided by the test section camera, which is overlooking the microtube and is protected by a watch glass. As seen from the video, a fireball is obtained at the tube failure condition. Three possible explanations are proposed to explain this explosive phenomenon, which was observed in all tests. First, the microtube could soften and fail mechanically, causing a hydrogen peroxide leak that would ignite in contact with air. Another explanation is that the microtube wall would partially fail, rapidly increasing its resistance and temperature, which would in turn ignite the hydrogen peroxide. Finally, the explosion could be simply due to the high local temperature at the microtube wall, which would trigger a decomposition reaction violent enough to cause a hydrogen peroxide explosion. Because of the low temperatures measured in the present series of tests (< 350°C) and because the microtube's mechanical integrity has been confirmed by Joppin [12] for temperature as high as 600°C, the latter explanation seems to be the most probable. Although no solid

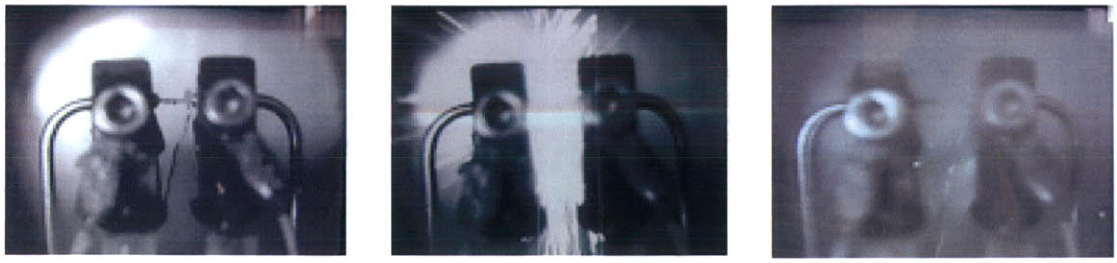

Figure 4-2: Test section explosion sequence from left to right. The above pictures correspond to three consecutive video frames separated by 1/24 s . Note that the combustion products fog the camera lens in the third frame.

proof has been provided here, this explanation is consistent with what is found in the literature [22,35] and therefore, for the present series of heat transfer experiments, the tube failure was assumed to be directly associated with a hydrogen peroxide explosion.

In addition to the measurement of pressure, mass flow and power supply, the outside wall temperature measurement is of great importance for deriving experimental results. Figure 4-3 shows the time evolution of the outside wall temperature measurement at the exit point on microtube, which was found experimentally to be the hottest. By comparing it with the power trace of Figure 4-1, the proportionality between this measurement and the power supplied is easily notable. Also shown on Figure 4-3 is the time evolution of the calculated inside wall temperature and exit bulk fluid temperature. For those two parameters, an increase proportional to the power dissipated is observed until failure occurs at 517 s. For this particular test, the inside wall temperature and consequently the local hydrogen peroxide temperature reached a maximum of approximately 146°C. Similar test results have been obtained for different mass flow and pressure conditions, the details of which will be discussed in the following sections.

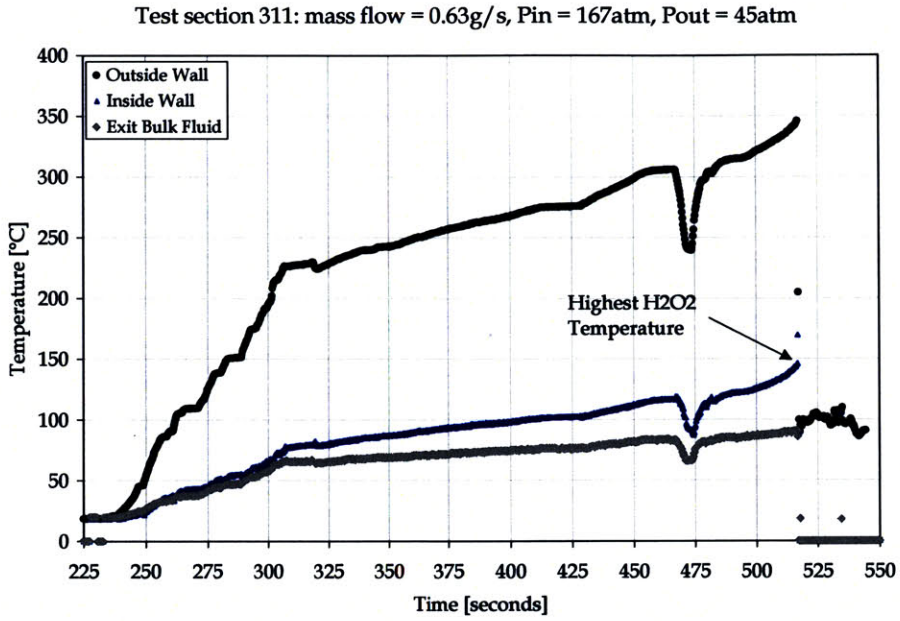

Figure 4-3: Typical exit temperatures evolution. Maximum outside wall temperature, inside wall temperature and fluid exit bulk temperature vs. time for test section 311.

4.2 Heat Transfer Test Results

The heat transfer test results with 98% hydrogen peroxide are presented here for each of the important quantities derived in section 3.4 . Parameters such as heat load, fluid bulk temperature, inside wall temperature and heat transfer coefficient are obtained at the microtube failure point or more specifically, at the last time sample available prior to failure. For each parameter, a brief discussion is also included and links the experimental results with the relevant theory presented in chapter 2.

4.2.1 Maximum Heat Load

As plotted in Figure 4-1, the maximum heat load is the power supplied or dissipated that triggers a hydrogen peroxide explosion. The effect of hydrogen peroxide pressure and mass flow on the maximum allowable heat load have been investigated and are presented in the following sub-sections.

4.2.1.1 Effect of Pressure

Table 4-1 shows the test results for 2 pairs of heat transfer tests done at similar mass flows but at considerably different pressures. As shown in Table 4-1, the exit pressure is 217.7 atm for test number 321 whereas for test number 313, it much lower at 38.2 atm. In addition, both tests are done at very similar mass flows and the fluid is supercritical in pressure, for test number 321. From these results, it can be seen that despite the significant difference in pressure, the power dissipated at failure is the same for both tests. This suggests that even a pressure level as high as the critical pressure of hydrogen peroxide has no effect on the maximum allowable heat load. The same conclusion can be drawn by looking at the experimental results for tests 324 and 325.

Test Number	P_{in} [atm]	P_{out} [atm]	$\dot{m}$ [g/s]	Q_{diss} [W]
321	294.3	217.7	0.374	62.3
313	81.5	38.2	0.379	64.0
324	281.7	217.2	0.462	87.9
325	136.4	70.4	0.466	91.3

Table 4-1: Experimental data prior to microtube failure for 4 different tests.

In retrospect, the independence of the maximum allowable heat load on pressure is not surprising. The explosion is a result of the thermally-induced decomposition of hydrogen peroxide, which is governed by an equation of the Arrhenius form. From equation 2.2, the reaction rate has been shown to be a function of the activation energy and temperature, but not pressure. Consequently, the results are consistent with the Arrhenius equation and pressure can be said to have negligible effects on the maximum allowable heat load in hydrogen peroxide cooling. Now that the effects of pressure have been assessed, the effects of flow velocity or mass flow on the maximum allowable heat load will be presented.

4.2.1.2 Effect of Mass Flow

Figure 4-4 shows the maximum allowable heat load as a function of mass flow, for the 13 heat transfer experiments performed. In the figure, two power quantities are presented: the power supplied and the power dissipated. As defined in section 3.4.4, the power dissipated is obtained by scaling the power supplied with the ratio of the microtube resistance and the assembly resistance. In effect, the power dissipated represents the power supplied minus the losses and is therefore, the appropriate quantity when defining the maximum allowable heat load.

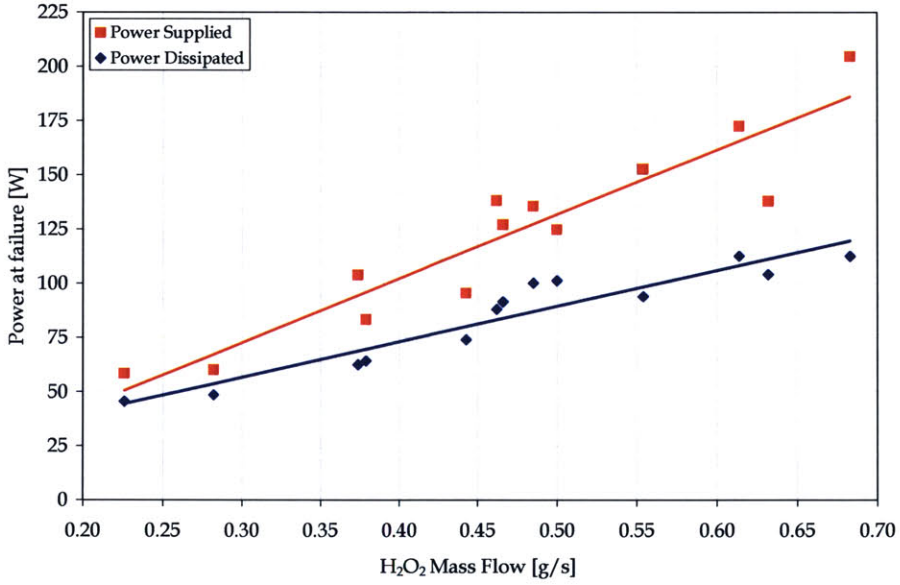

Figure 4-4: Power supplied and power dissipated vs. H_2O_2 mass flow rate. Maximum achievable heat loads prior to microtube failure, for all mass flows tested.

Althought the above power scaling is an idealization, confidence in the calculation can be gained by considering the two tests cases with a mass flow of approximately 0.37 g/s, plotted on Figure 4-4. As these two tests demontrate, their power supplied are quite different but their power dissipated are very similar. By looking at the data more closely, this difference in power supplied was due to varying electrical connection quality between the two tests. Accordingly, the power scaling produces more repeatable results by removing the electrical connection variability. As a result, the power supplied data

will not be used any further in this thesis and is provided in Figure 4-4 only as a reference.

The increase in maximum heat load with hydrogen peroxide mass flow, observed in Figure 4-4, is consistent with what is expected from theory. From a simple energy balance, the bulk temperature rise ΔT_b of a fluid is given as follows:

$$T_b\ (in) - T_b(out) = \Delta T_b = \frac{Q_{DISS}}{\dot{m}\, Cp} \tag{4.1}$$

where ΔT_b is the bulk temperature rise in °C, Q_{DISS} is the power dissipated in Watts, $\dot{m}$ is the mass flow in kg/s and Cp is the heat capacity in J/kg-K .

Assuming the explosion phenomenon only allows a fixed hydrogen peroxide bulk temperature rise for a given tube size (to be shown in the next section), an increase in power dissipated is expected for a corresponding increase in mass flow. Moreover, equation 4.1 states that this relationship should be linear. As a result, a least square linear fit has been added to Figure 4-4 and represents the phenomenon fairly well, even if the exact physical details are more involved.

4.2.2 Bulk Temperature

Figure 4-5 shows the maximum achievable bulk temperature at the exit plane of the microtube, as a function of mass flow. As can be seen from the plot, the test results obtained with the 95.5 µm tube suggest that the exit bulk temperature at failure is independent of mass flow and equal to approximately 99°C. To confirm those results, a series of 3 heat transfer tests have been carried in 194 µm tubes, with the same procedure. For those 3 tests, the exit bulk temperature was found to be much lower than previous test, at approximately 50°C. Although this confirms the independence of exit bulk temperature on mass flow, it reveals that this value is size specific. Fortunately, this

phenomenon is expected and can be explained by the fact that the sharp temperature profile near the wall occupies less height in a large diameter tube. Therefore, the mass average of the temperature profile (bulk temperature) is lower in a larger tube, assuming constant wall temperature (to be shown in the next section).

From the above discussion, the dependence of bulk temperature on tube size is fairly obvious. Because of this dependence, its value cannot be the hydrogen peroxide instability criterion sought in this thesis. Instead, a maximum local fluid temperature is preferred and is presented below.

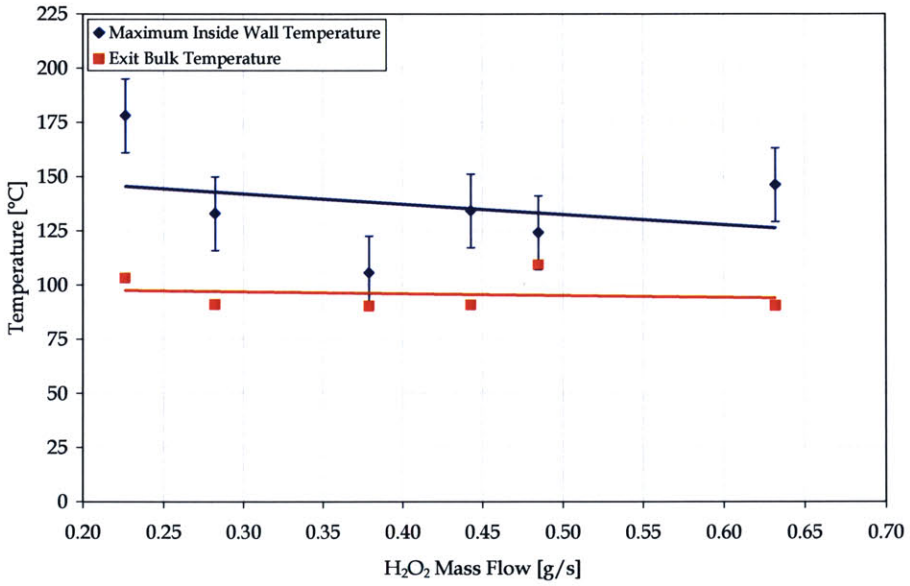

Figure 4-5: Inside wall temperature and corresponding exit bulk temperature vs. H_2O_2 mass flow rate. Maximum achievable temperatures prior to microtube failure, for all mass flows tested.

4.2.3 Maximum Inside Wall Temperature

In the current experiment, the highest local temperature reached by hydrogen peroxide is found at the microtube exit plane on the inside wall interface. Because the hydrogen peroxide explosion phenomenon is local and temperature dependent, the maximum inside wall temperature is considered a logical choice for the instability criterion. Accordingly, Figure 4-5 shows the results for this maximum inside wall temperature as

a function of mass flow. As can be seen from the figure, results suggest that a local temperature in the range 125°C-150°C will cause a hydrogen peroxide explosion. In addition, this is independent of size as confirmed by the 3 experiments done with the larger microtubes. Despite the large uncertainty in the results, due mostly to the variability in outside wall temperature measurement, the range shown in Figure 4-5 is consistent with the 150°C found in previous hydrogen peroxide stability studies [35].

The theoretical justification for the hydrogen peroxide instability limit of 150°C is not clear. However, as previously shown in Figure 2-3, vapor explosion boundary data suggest 126°C as the highest temperature allowed at 2 atm [34]. The effects of pressure having been found to be negligible, an instability limit of 150°C is thus not inconceivable. In addition to the actual value of the limit, the mechanism for thermally induced decomposition of hydrogen peroxide leading to an explosion is not well understood. A simple explanation for the phenomenon is given by Mok et. al. [22] which suggests that "if a concentrated aqueous hydrogen peroxide solution is heated to a temperature at which the vapor produced lies within the explosive composition range, it is possible to ignite the vapor ... with a spark, a hot wire, or a catalytically-active surface". For pressures above the critical point, they state that "the liquid phase decomposition could cause very high local heating rates and possibly explosive gasification".

The above quotes suggest that, in the present heat transfer experiments, the hydrogen peroxide vapor is ignited by a catalytically active surface. Accordingly, improvements in stability might be possible when hydrogen peroxide is used in the micro-rocket silicon cooling channels, instead of the stainless steel microtubes. Although they have been passivated, the 304 stainless steel walls are made of class 2 material and have some degree of surface catalysis. On the other hand, the silicon cooling passages would be covered with a protective silicon oxide barrier (SiO_2) which would reduce surface activity. Consequently, by using a class 1 surface material and eliminating the silver solder contaminant of the current microtubes, silicon channels might improve the

hydrogen peroxide thermal stability. Because such improvements are hard to quantify at this point, heat transfer tests in silicon microtubes are judged necessary and should be conducted before the final design phase of the micro-rocket engine.

4.2.4 Heat Transfer Coefficient

Another parameter of interest when designing the cooling passages is the convective heat transfer rate allowed by flowing hydrogen peroxide. Factors such as the scale, the decomposition reaction and the limited amount of thermo-physical properties available for hydrogen peroxide can greatly affect the heat transfer rates predicted with standard correlations. Consequently, this sub-section investigates the validity of those correlations by comparing them with a forced convective heat transfer coefficient obtained experimentally.

The following usual definitions are used in the rest of this chapter:

$$Nu_D = \frac{hD}{k_f} \qquad \mathrm{Re}_D = \frac{\rho UD}{\mu} \qquad \mathrm{Pr} = \frac{\mu Cp}{k_f} \tag{4.2}$$

where Nu_D corresponds to the Nusselt number, Re_D to the Reynolds number, Pr to the Prandtl number, ρ is the density in kg/m^3, μ is the viscosity in Ns/m^2, k_f is the thermal conductivity of the fluid in W/m-K, Cp is the specific heat in J/kg-K, h is the heat transfer coefficient in J/m^2-K and D is the microtube inside diameter in m.

4.2.4.1 Standard Correlations

The results for the forced convective heat transfer coefficient obtained experimentally will be compared with the following correlations:

Colburn Correlation [15]

$$Nu_D = 0.023\,\mathrm{Re}_D^{\,0.8}\,\mathrm{Pr}^{1/3} \tag{4.3}$$

The fluid properties are evaluated at the film temperature:

$$T_f = (T_b + T_w)/2 \tag{4.4}$$

This macro-scale correlation applies for turbulent flow in smooth pipes in the range $6{,}000 \leq \mathrm{Re}_D \leq 300{,}000$ and has a quoted accuracy of ±40% for $0.67 \leq \mathrm{Pr} \leq 100$.

Gnielinski Correlation [15]

$$Nu_D = \frac{(f/8)(\mathrm{Re}_D - 1000)\,\mathrm{Pr}}{1 + 12.7\sqrt{f/8}\,(\mathrm{Pr}^{2/3} - 1)} \tag{4.5}$$

The fluid properties are evaluated at the fluid bulk temperature and the friction factor for smooth pipes is given by:

$$f = \frac{1}{(1.82\log_{10}\mathrm{Re}_D - 1.64)^2} \tag{4.6}$$

This macro-scale correlation applies for transitional and turbulent flow in smooth pipes in the range $2{,}300 \leq \mathrm{Re}_D \leq 500{,}000$ and has a quoted accuracy of ±6% for $0.5 \leq \mathrm{Pr} \leq 200$.

Microtube Correlation [32]

In general, for fluid flow in microtubes, the Nusselt number obtained experimentally is much higher than the one predicted by conventional macro-scale correlations. Yu et. al. [32] confirmed that observation with a series of heat transfer tests in 19, 52, and 102 μm tubes using nitrogen gas and water. As a result of their experimental and theoretical investigation, they suggest the following modified form of the Colburn correlation:

$$Nu_D = 0.007\,\mathrm{Re}_D^{1.2}\,\mathrm{Pr}^{0.2} \tag{4.7}$$

As for the standard macro-scale correlation, the fluid properties are evaluated at the film temperature. This correlation is valid for turbulent flow in microtubes with a Reynolds

number range of 6,000 ≤ Re_D ≤ 20,000. The accuracy is unknown and the range of Prandtl number tested was 0.7 ≤ Pr ≤ 5.

4.2.4.2 Experimental Results

For the present hydrogen peroxide study, the tested range of Reynolds number varied from approximately 4,800 to a maximum of 16,000. In addition, for a temperature range of 20 to 80°C, the Prandtl number for hydrogen peroxide varies from 2.5 to 5.2. For the most part, this is within the range of validity of the correlations presented in the previous section. Accordingly, Figure 4-6 compares the experimental heat transfer coefficient with those correlations. As can be seen from the figure, the uncertainty in the test data is rather large. This is mainly due to the uncertainty on the small geometry and to the large fluctuation between the inside wall and the bulk temperature data (see Figure 4-5). To reduce those fluctuations, a smooth experimental fit for the heat transfer coefficient has been obtained using a straight-line approximation for both, the inside wall temperature and the bulk temperature, as shown in Figure 4-5. The dark solid line on Figure 4-6 represents this experimental fit obtained for the heat transfer coefficient as a function of mass flow. The results plotted in Figure 4-6 show that standard macro-scale correlations such as Gnielinki and Colburn significantly underestimate the heat transfer coefficient whereas the Microtube correlation overestimates the heat transfer coefficient. Nonetheless, these correlations could be used as upper and lower bounds in hydrogen peroxide forced convective cooling.

4.3 Summary

This chapter has presented and discussed the results obtained for the 98% liquid hydrogen peroxide heat transfer tests. The primary conclusions are as follows:

- For a cooling passage, the thermally induced decomposition of 98% hydrogen peroxide leads to a maximum allowable heat load, which increases linearly with coolant mass flow.

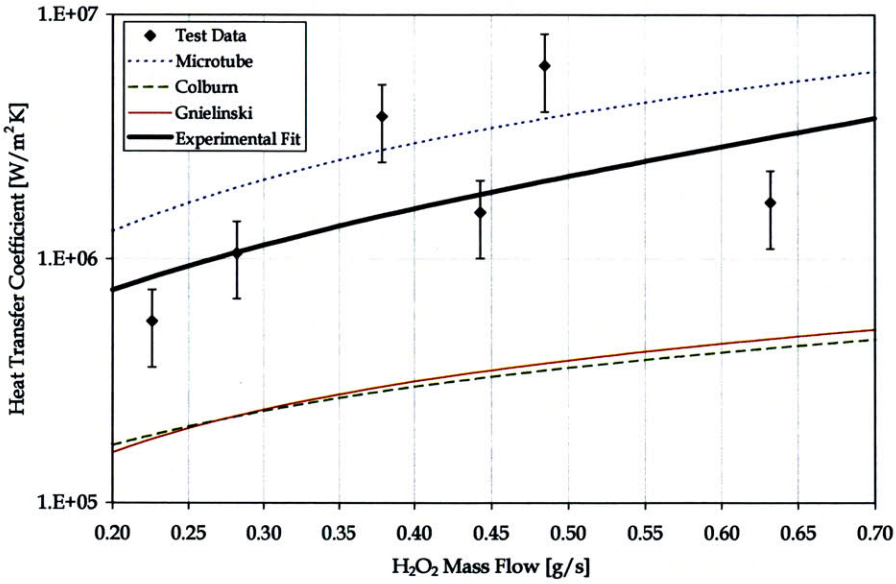

Figure 4-6: Forced convective heat transfer coefficient vs. H_2O_2 mass flow rate. Comparison between experimental data, experimental average, macro-scale correlations such as Gnielinski and Colburn, and a Microtube correlation.

- Independent of pressure, mass flow and tube size, a local fluid temperature or wall temperature of approximately 150°C consistently yields an explosion, in a 98% hydrogen peroxide passivated stainless steel cooling passage.

- Standard macro-scale correlations significantly underestimate the heat transfer coefficient achievable in a 98% hydrogen peroxide microtube. Although it overestimates the heat transfer, a micro-scale correlation is presented and provides a more accurate estimate.

Taken together, these results have a considerable impact on future designs of the micro-rocket engine. The next chapter will discuss this issue and will provide recommendations for future work.

Chapter 5

Conclusions and Recommendations

This chapter summarizes the research discussed in this thesis, concludes about the impact of the results on the design of the micro-rocket engine and provides recommendations for future work in this area.

5.1 Summary

The concept of MEMS-based micro-rocket engines has been presented and previous work on propellant analysis has been reviewed. From the selection of H_2O_2 as the oxidizer for the regeneratively-cooled micro-rocket engine, a hydrogen peroxide coolant study has been motivated. Following the framework established by Joppin [12], an experimental investigation of heat transfer to hydrogen peroxide has been initiated, with the objective of determining its decomposition stability limit at high temperature.

As part of this investigation, a literature review has been performed and the necessary background information on hydrogen peroxide's attractive features, thermo-physical properties, thermal decomposition reaction, safety and material compatibility, has been presented.

A test apparatus compatible with 98% hydrogen peroxide has been designed and built, based on the work of Lopata [19], Faust [8] and Joppin [12]. Such an apparatus of which the main component is a 95.5 μm inside diameter, 4 mm long, electrically heated stainless steel microtube, has been used to perform heat transfer tests with 98%

hydrogen peroxide at pressures, temperatures, heat fluxes and length scale relevant to the design of the micro-rocket engine.

As the major outcome of this study, the experimental data obtained from the heat transfer tests in stainless steel microtubes has been analysed and suggests that independent of pressure, mass flow and tube size, a local fluid temperature or wall temperature of approximately 150°C consistently yields an explosion, in a 98% hydrogen peroxide cooling passage.

5.2 Impact on the Design of the Micro-Rocket Engine

The experimental results presented in this study have a considerable impact on future designs of the micro-rocket engine. As mentioned above, independent of pressure, mass flow and tube size, results suggest that a local fluid temperature of approximately 150°C consistently yields an explosion in a 98% hydrogen peroxide stainless steel cooling passage. If this holds for silicon cooling passages as well, this would add a major constraint to the regenerative-cooling scheme and consequently, to the overall rocket cycle. Instead of the temperature rise of 510°C planned originally (see Figure 1-1), the portion of the cooling jacket using 98% hydrogen peroxide would benefit, at most, from a temperature rise of approximately 120°C [9]. With a design oxidizer to fuel ratio of approximately 4.1, where the 98% hydrogen peroxide constitutes most of the propellant flow, there would most likely not be enough cooling capacity in the propellants to cool the nozzle. Moreover, even if there were, the enthalpy gained by the 98% hydrogen peroxide flow would not be sufficient to drive its own turbopump [27]. Consequently, the intended H_2O_2/JP7 expander cycle presented in section 1.1.2 may not be achievable.

It should be clarified, however, that the results of this study do not eliminate the H_2O_2/JP7 propellant combination. As suggested by Protz [26], a decomposition topping

[9] This number assumes an initial propellant temperature of 25°C and a maximum bulk temperature limit of 145°C. This is judged the highest feasible temperature rise. As shown in previous sections, a passage diameter of 95 μm only allows for a 75°C temperature rise.

cycle is still possible and meets the pressure requirement of the system. Instead of using an enthalpy increase to run the turbopump, this cycle intentionally destabilizes the 98% hydrogen peroxide in a decomposition chamber and runs both turbopumps with the decomposition products. Figure 5-1 shows the hydrogen peroxide flow circuit for such a cycle. As can be seen from the figure, the hydrogen peroxide first regeneratively-cools the nozzle, then flows through a catalyst bed to accelerate its decomposition and is finally injected into the combustion chamber, after exiting the turbine. As pointed out by Protz [26], this cycle has the advantage of decoupling the pump performance from the cooling system design. However, it has two drawbacks in that it requires an extra decomposition chamber, and only one of the two propellants drives the pumping system.

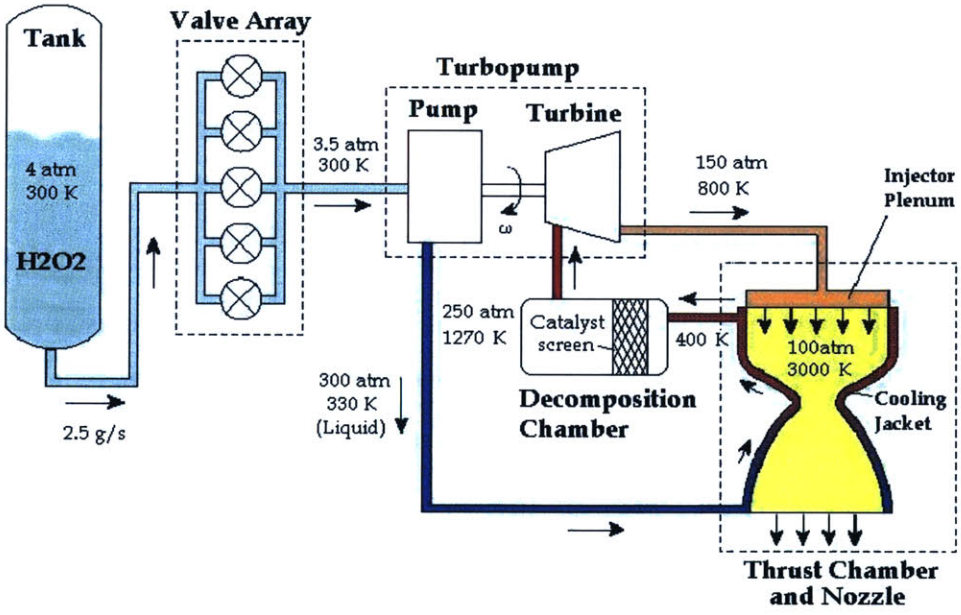

Figure 5-1: Example of hydrogen peroxide decomposition topping cycle for future designs of the micro-rocket engine (only one propellant line shown).

5.3 Recommendations for Future Work

For the current study, heat transfer tests have been performed mainly with 95.5 μm inside diameter microtubes. To evaluate the effects of tube size on the results, three additional tests were performed using bigger tubes, with a 194 μm inside diameter.

Although results do not show any major differences, a more thorough investigation of the effects of tube size on hydrogen peroxide's thermal stability limit should be done. Because the H_2O_2/JP7 micro-rocket engine will use cooling passages with hydraulic diameters of approximately 20 μm at the throat [13], heat transfer tests with smaller diameter microtubes might prove useful in predicting the cooling behavior of hydrogen peroxide in the actual engine.

More important than the tube size, the microtube's material of construction should be changed to reflect the actual surface conditions found in the micro-rocket engine. As mentioned in chapter 4, improvements in stability might be possible when hydrogen peroxide is used in the micro-rocket silicon cooling channels, instead of the stainless steel microtubes. Current understanding of the phenomenon suggests that a protective silicon oxide barrier (SiO_2), which would be grown on the passage wall, would reduce the surface activity and improve the hydrogen peroxide thermal stability [22]. Because such improvements are hard to quantify at this point, heat transfer tests in silicon microtubes should be conducted before the final design phase of the micro-rocket engine. In addition to more adequately replicating the wall surface conditions of the engine, such a silicon microtube would have the benefit of being mass-producible, of using a lower control current enhancing safety, and would allow for more geometrical flexibility and simplicity.

Finally, as suggested by Joppin [12] and Protz [27], it would be interesting to test hydrogen peroxide in the current gaseous micro-rocket engine. Such an experiment would validate the stability limit determined with the stainless steel microtubes, and would assess the prediction made in this thesis for the heat transfer coefficient achievable in hydrogen peroxide micro cooling passages.

Appendix A

Uncertainty Analysis

A.1 Introduction

This appendix presents an analysis of the uncertainty associated with the results derived in this thesis. In the first section, the uncertainty associated with the independent measurements is presented. In the second section, the uncertainty associated with the derived quantities due to uncertainty propagation is presented in details. At the end of this section, a brief comment is made about the impact of uncertainty on the results derived in this thesis [12].

Throughout Appendix A, a quantity with uncertainty is noted as follows:

$$\widetilde{x}_i = x_i \pm dx_i \tag{A.1}$$

where $\widetilde{x}_i$ is a numerical quantity that can be represented by its main part or sensor reading x_i and its associated uncertainty dx_i.

A.2 Uncertainty Associated with Independent Measurements [12, 17]

A.2.1 Pressures

The calibration of the pressure transducer was done using a Heise gauge which has a stated accuracy of ±0.25% with a pressure range of 0 to 6000 psi. This corresponds to a reference pressure accuracy of ±15 psi. The pressure transducers have a BLSF (Best Line

Straight Fit) accuracy of ±0.4% for the 0-5000 psi range. In addition, measurement fluctuations as large as ±2.3 psi were recorded during testing. Therefore, the estimation of uncertainty for the pressure measurements is as follows:

$$dP = \pm(15 + 20 + 2.3) = \pm 37\,psi \quad or \quad \pm 2.5\,atm \tag{A.2}$$

For a typical inlet pressure of 1,600 psi, this corresponds to an uncertainty of ±2.3%.

A.2.2 Mass Flow

The hydrogen peroxide mass flow is measured with a factory calibrated CFM010P MicroMotion Elite sensor. For the mass flow range considered in this thesis (0.2 - 0.8 g/s) it has an estimated accuracy no worse than ±0.002 g/s. During testing, fluctuations as large as ±0.005 g/s were observed at steady-state. Therefore, the estimation of uncertainty for the hydrogen peroxide mass flow measurement is as follows:

$$d\dot{m} = \pm 0.007\,g/s \tag{A.3}$$

For a typical mass flow of 0.5 g/s, this corresponds to an uncertainty of ±1.4%.

A.2.3 Power Supplied

The power supplied to the test section is the product of a current and voltage measurement. The current is measured using a 0-150 Amps shunt, which a calibrated accuracy of ±0.5%. Because the voltage is directly fed in a high impedance data acquisition module, the uncertainty on the voltage is considered negligible. In addition, reading fluctuations as large as ±0.07 Amps and ±0.002 Volts were observed, respectively, for the current and voltage measurements. Therefore, the estimation of uncertainty for the current and voltage measurements is as follows:

$$dI = \pm(0.75 + .07) = \pm 0.82 Amps \quad \text{(A.4)}$$

$$dV = \pm 0.002 Volts \quad \text{(A.5)}$$

For typical values of 47.1 Amps and 2.876 Volts, this corresponds to uncertainty values of ±1.7% and ±0.07%, respectively.

A.2.4 Main Tank Temperature Measurement

The fluid temperature in the main tank is measured with T-type Omega thermocouple dipped into the fluid. It has a stated accuracy of ±1°C and a measurement variation during testing as large as ±0.2°C. Therefore, the estimation of uncertainty for the main tank temperature measurement is as follows:

$$dT_{TANK} = \pm 1.2°C \quad \text{(A.6)}$$

For a typical fluid temperature of 20°C, this corresponds to an uncertainty of ±6%.

A.2.5 Outside Wall Temperature Measurement

Because it has not been used extensively in this thesis, the uncertainty in infrared sensor reading is not developed here. Instead, the estimation of the uncertainty for the outside wall measurement is adapted from Joppin [12] and is presented as:

$$dT_o = \pm(0.055T_o + 30)°C \quad for \ T_o < 450°C \quad \text{(A.7)}$$

$$dT_o = \pm(0.055T_o + 25)°C \quad for \ T_o > 450°C \quad \text{(A.8)}$$

Another outside wall temperature measurements was also obtained with a K-type thermocouple which as a stated accuracy of ±1°C. For this measurement, an additional uncertainty is introduced due to the ceramic layer between the thermocouple and the tube surface. Since this uncertainty is hard to estimate, 3% of the temperature reading

was chosen as an upper limit. Finally, measurement fluctuations as large as ±0.35°C were observed during tests. Considering all those uncertainties, the estimation of uncertainty for the outside wall temperature measurement is as follows:

$$dT_o = \pm(0.03T_o + 1.35)°C \tag{A.6}$$

For a typical outside wall temperature of 320°C, this corresponds to an uncertainty of ±3.4%.

A.2.6 Tube Dimensions

Given the importance of the tube dimensions in the data reduction and the fact that they were obtained experimentally, a complete discussion of the tube dimensions and their uncertainty was included in section 3.3.3 . The results of that discussion were presented in Table 3-1 where the uncertainty of the microtube inside diameter, microtube outside diameter and resistive length were given as ±1.5 μm, ±4 μm and ±0.05 mm respectively.

A.2.7 Tube Resistance

The microtube resistance is measured experimentally before each test and is used in equation 3.4 to obtain the fraction of the heat dissipated by resistive heating. On average, a tube resistance of 40 mΩ has been measured at room temperature with a variation of 1.5 mΩ between tubes. Furthermore, from the properties of 304 stainless steel and the uncertainty in tube geometry, the uncertainty in microtube resistance was evaluated and was found to be 1.6 mΩ. This then confirms the geometrical uncertainty values presented above.

A.2.8 Temperature Measurement Position

The uncertainty associated with the position x, where the thermocouple and infrared sensor temperature measurements are taken, has an influence on the radial power balance at the end of the tube. For the sensor, the uncertainty comes from the ±0.05 μm stage drift and from the initial misalignment. This has been evaluated by Joppin at ±25

μm [12]. For this analysis, the thermocouple measurement is assumed to have twice this positional uncertainty:

$$dx = \pm 0.05mm \tag{A.10}$$

For a typical end of tube position of 3.65 mm, this corresponds to an uncertainty of ±1.4%.

A.3 Uncertainty Associated with Derived Quantities [12, 17]

The uncertainty of each of the derived quantities is propagated from the uncertainty in the independent measurements as follows. Let y be a quantity derived from the independent measurements $x_1, x_2, ..., x_n$.

$$y = f(x_1, x_2, ..., x_n) \tag{A.11}$$

From calculus, the uncertainty $d\hat{y}$ is defined as:

$$d\hat{y} = \sum_{i=1}^{n} \left(\left. \frac{\partial f}{\partial x_i} \right|_{(x_1, x_2, ..., x_n)} dx_i \right) = \sum_{i=1}^{n} C_i dx_i \tag{A.12}$$

where dx_i is the uncertainty of the ith measurement and C_i is the dimensional sensitivity of the derived uncertainty $d\hat{y}$ with respect to the ith measurement x_i.

To avoid the possibility of negative sensitivities and to average out the contributions of each measurement x_i, an engineering uncertainty is defined as:

$$dy = \pm \sqrt{\sum_{i=1}^{n} (C_i dx_i)^2} \tag{A.13}$$

The rest of this section presents the uncertainty associated with the derived quantities for three representative test cases [12]. The selected cases cover the entire range of measurements obtained in this thesis and are summarized in Table A-1.

Parameters	Case 1	Case 2	Case 3
$\dot{m}$ [g/s]	0.23	0.44	0.63
Q [W]	58.4	95.6	137.9
x [mm]	3.65	3.65	3.65
T_o [°C]	266	280	345

Table A-1: Cases selected for the uncertainty analysis.

For the derived quantities presented below, the partial derivative with respect to each measurement was taken according to equation A.12. Then, the engineering uncertainty was computed using equation A.13 and the modeling uncertainty was added when applicable.

A.3.1 Power Supplied

Parameters	Case 1	Case 2	Case 3
Q [W]	58.4	135.6	137.9
dQ [W]	1.5	1.9	2.4
dQ [%]	2.6%	2.0%	1.7%

Table A-2: Uncertainty in power supplied for three cases.

A.3.2 Electrical Resistance of the Assembly

Parameters	Case 1	Case 2	Case 3
R_{TOTAL} [mΩ]	57.9	54.4	59.7
dR_{TOTAL} [mΩ]	1.5	1.1	1.0
dR_{TOTAL} [%]	2.6%	2.0%	1.7%

Table A-3: Uncertainty in electrical resistance of the assembly for three cases.

A.3.3 Power Dissipated

Parameters	Case 1	Case 2	Case 3
Q_{DISS} [W]	45.4	73.8	103.9
dQ_{DISS} [W]	2.2	3.3	4.3
dQ_{DISS} [%]	4.8%	4.5%	4.1%

Table A-4: Uncertainty in power dissipated for three cases.

A.3.4 Bulk Temperature

Parameters	Case 1	Case 2	Case 3
$T_b(x)$ [°C]	103.2	90.8	90.4
$dT_b(x)$ [°C]	2.6	3.8	3.5
$dT_b(x)$ [%]	2.5%	4.1%	3.9%

Table A-5: Uncertainty in exit bulk temperature for three cases.

A.3.5 Inside Wall Temperature

Parameters	Case 1	Case 2	Case 3
T_i [°C]	178	134	146
dT_i [°C]	11	13	17
dT_i [%]	6%	10%	12%

Table A-6: Uncertainty in inside wall temperature for three cases.

The uncertainty in the inside wall temperature are fairly large, reaching as high as 12% in one case. However, this is expected given the large number of parameters involved in the calculation. A sensitivity study was carried out and shows that half of the uncertainty is a direct consequence of the outside wall temperature measurement. Despite the uncertainty of ±17°C, the experiment yields a satisfactory estimate for the maximum temperature achievable with hydrogen peroxide.

A.3.6 Heat Transfer Coefficient

Parameters	Case 1	Case 2	Case 3
h [10^5 W/m^{2}K]	5.5	15.5	17.1
dh [10^5 W/m^{2}K]	1.0	5.2	5.5
dh [%]	18%	34%	32%

Table A-7: Uncertainty in heat transfer coefficient for three cases.

As can be seen from Tables A-7, the uncertainty in the convective heat transfer is fairly large. This is expected since its calculation involves a relatively small difference between two large temperature values. Because of that, uncertainties as high as 35% have been reached. Consequently, the experiment provides, at best, an order of magnitude estimate on the force convective heat transfer rate achievable in hydrogen peroxide.

Appendix B

Experimental Checklist

This appendix shows a copy of the three experimental checklist used in running a hydrogen peroxide heat transfer test. The first checklist, shown in Figure B-1, is used for test cell preparation, instrument check and initial system purge. The second checklist is used for hydrogen peroxide transfer, for testing, for purging the rig after a test and as a safety check before returning to the test cell. The last checklist, shown in Figure B-3, is used for the final water purge procedure and for the system shutdown.

H2O2 Heat Transfer Rig, Prepare Test Cell Checklist (CL1)
Last Update: 2/24/2004

Date: ____
Time: ____
Who: ____

	Action	Notes:
	System Preparation	
☐	Put on gloves and glasses	
☐	Close Rocket Test Stand O2 pump supply	
☐	Switch OFA to Heat Transfer Rig	
☐	Switch He to H2O2 Rig Purge Tank	
☐	Close manual He vent in control room	
☐	Close purge line vent in control room	
☐	Plug pneumatic valves cable to power outlet	
☐	Open water hose valve	
☐	Turn on OFA compressor	
☐	Open "Oriel_motor_mathieu" DAS in Labview	
☐	Run "Relays Only" control in Labview	
☐	Run "Measurement_no_saving" in Labview	
☐	Verify Oil-free Air at pressure	pressure: ____
☐	Open OFA to control valves	
	Prepare Purge System and Drains	
☐	Verify deionized water level in purge tank	
☐	Close purge tank vent	
☐	Put 3-way valve in neutral position	
☐	Verify Focus of Drain Camera & light	
☐	Attach bypass section on rig	
	Electronics	
☐	Turn on flowmeter supply	
☐	Turn on IR sensor supply	
☐	Turn on pressure transducer supply to 15V	
☐	Turn on power to relays	
☐	Verify relays work	
	Prepare portable tank for filling	=> careful, H2O2 trapped in the ball valv
☐	Flush tank with water	
☐	Vaccum tank	
☐	Unscrew funnel	
☐	Bring tank to fume hood stand	
	Purge H2O2 Residual Vapor / water	
☐	Pressurise Main Tank to ~ 60psi	=> open the valve before the regulator
☐	Cycle each valves	
☐	Purge system with He	
☐	Set the 3 PP containers with water under the drains	
	Dump tank filling	
☐	Vacuum dump tanks	
☐	Fill the dump tank with water	volume: ____
☐	Close manual valve	
☐	Set dump tank choked orifice (~1/100 turn)	
	Test Section Alignment	
☐	Attach test section & heat flux cables	number: ____
☐	4-wire resistance measurement	start pos: ____
☐	Attach TC and Put the protective PP with water	res_tube: ____
☐	Verify Focus Test Section Camera	res_asmby: ____
☐	Verify alignment with light	TC_pos: ____
☐	Set the zero	
☐	Scan the microtube	
	Final Alignment Test	
☐	Insert fiber optic cable in IR sensor	
☐	Set Oriel control to "Remote"	

Table B-1: Prepare test cell checklist.

H2O2 Heat Transfer Rig, Test Procedure Checklist (CL2)
Last Update: 2/24/2004

Date:
Time:
Who:

	Action	Notes:
	Bring H2O2 to test cell	
☐	Put on the PVC suit and face sheild	
☐	Measure H2O2 volume	volume:
☐	Fill removable tank	
☐	Close all manual valves	
☐	Rinse outside with water	
☐	Bring to test cell and attach teflon hose & Thermocouple	
☐	Open tank vent and bottom valve	
☐	Connect Main Tank Thermocouple	
☐	Close door and move to control room	
☐	Verify Labview parameters: filenames, maximum flow, density, travel step	
☐	Place DO NOT ENTER SIGN on the door	filename:
	Main Tank Filling	
☐	Open He vent	
☐	Allow H2O2 Transfer (wait 1.5 min)	
☐	Disable H2O2 Transfer	
☐	Close He vent	
☐	Stop all running programs	
	TESTING	test goal:
		run time:
☐	VCR On	
☐	Run "Oriel_motor_mathieu" DAS in Labview	
☐	Run "Relays Only" control in Labview	actual / target
☐	Pressurize main tank	pressure:
☐	Pressurize dump tank	pressure:
☐	Open flow valve, record mass flow	mdot:
☐	Set maximum mass flow	max mdot:
☐	Enable HP Power supply	
☐	Ramp up heat flux	V, A :
☐	Wait for steady-state	
☐	Press "Save" to start motor carriage	
	End of experiment	
☐	Turn off HP Power supply	
☐	Close Main Flow valve	
☐	Back off regulators	
☐	Data saved ?	
☐	Stop "Oriel_motor_mathieu" DAS	
☐	Test Section Mechanical Integrity ?	
	Purge system of H2O2	
☐	Open Main Tank He vent (plug ears)	
☐	Open Drain 2	
☐	Vent Dump Tank & Open Drain 3	
☐	Pressurize Dump Tank to 50 psi	
☐	Open Main Flow valve	=> H2O2 in test section region
☐	Open Drain 1	should be dripping
☐	Open Fill valve and let all H2O2 drain	=> all H2O2 should be dripping
☐	Close All valves	
☐	Pressurize Main Tank to 25psi	=> open drain first
☐	Cycle Drain 1	
☐	Cycle Drain 2	
☐	Open Drain 3	
☐	Cycle Main Flow valve	
☐	Pressurize Dump Tank to 100psi	
☐	Back off regulators	
☐	Close All valves	
☐	Vent Main Tank	

Table B-2: Test procedure checklist.

H2O2 Heat Transfer Rig, Return to Test Cell Checklist (CL3)
Last Update: 2/24/2004

Date: ____
Time: ____
Who: ____

	Action	Notes:
	Initial Water Purge	
☐	Open Purge He bottle	
☐	Open Drain 2	
☐	Pressurize Main Tank to ~20 psi	
☐	Open Purge Valve	
☐	Pressurize Purge Tank until water flows	=> Look for mass flow reading
☐	Close Drain 2	
☐	Open Drain 3 + Main Flow valve	=> Look for mass flow reading or water in PP containers
☐	Close Drain 3 + Main Flow valve + Purge valve	
☐	Back off regulators	
☐	Vent Purge Tank	
☐	Vent Main Tank	
☐	Open all valves and let water drain	
	Return to Test Cell	
☐	HP Power supply off ?	
☐	Open all valves except purge	
☐	All Temperature OK?	temp: ____
☐	Spray the outside of the of the PP with water	
☐	Empty the PP containers	
☐	Attach bypass section on rig	
☐	Close needle valve	
	Final Water Purge	
☐	Open Drain 2	
☐	Pressurize Main Tank to ~20 psi	
☐	Open Purge Valve	
☐	Pressurize Purge Tank until water flows	=> Look for mass flow reading
☐	Close Drain 2	
☐	Open Drain 3 + Main Flow Valve	=> Flow water for 30 sec
☐	Close Drain 3 + Main Flow valve + Purge valve	
☐	Back off regulators	
☐	Vent Purge Tank	
☐	Vent Main Tank	
☐	Open all valves and let water drain	
	Purge residual water in rig	
☐	Open Drain 1, pressurise until empty	
☐	Open Drain 2, pressurise until empty	
☐	Open Drain 3 + main flow, pressurise until empty	
☐	Vent Main Tank	
☐	Open Drain 3, pressurise exhaust tank	
☐	Close all valves	
☐	Open fill valve + Drain 1	
☐	Flow water through Fill Tank	=> careful, H2O2 trapped in the ball valv
☐	Empty the 3 PP containers	
	System Shutdown	
☐	Close the 2 He bottles	
☐	Vent Main Tank He line	
☐	Vent Dump Tank He line	
☐	Vent Purge Tank He line	
☐	Vent OFA line	
☐	Close water hose	
☐	Turn off the IR Power Supply	
☐	Turn off the flowmeter power supply	
☐	Turn off the power to pressure transducer	
☐	Turn off power to valves solenoids	
☐	Switch He valve to Rocket Test Stand	
☐	Close all valves on Fill Tank	
☐	Close OFA supply in test cell	
☐	Turn off the OFA compressor	
☐	Dilute and dispose of waste H2O2	

Table B-3: Return to test cell checklist.

Appendix C

List of parts

This appendix lists the parts used in the current test rig that have been found compatible with 98% hydrogen peroxide after proper passivation.

Part Name	General Description	Brand	Ordering Number
Dump Tank	316L SS Tank - 500mL	Swagelok	316L - 50DF4 - 500
Fill Tank	316L SS Tank - 1000mL	Swagelok	304L - HDF4 - 1000
Pneumatic Valves	316 SS 83 Series Trunnion Ball Valve with actuators	Swagelok	SS-83KS4-31CD SEAT PCTFE
2 & 3-way Manual Ball Valves	316 SS 83 Series Trunnion Ball Valve	Swagelok	SS-83XKS4 SEAT PCTFE
Manual Needle Valves	316 SS 1 Series Needle Valves, regulating stem	Swagelok	SS-1RS4
Check Valves	316 SS CH Series Valve, Cracking P=25psi	Swagelok	SS-CHS4-25
Burst Disk Unit	ST Screw Type Holder with SCRD Rupture disk, BP 5000psig	Fike	SCRD DN15 1/2" ST FS, ST Holder 1/2"
Main Tank O-Ring	321 SS Teflon® coated o-ring	American Seal & Eng.	12-03562-I31-T2
Fluorolube	Fluorolube GR-362	Gabriel Performance	GR-362
Flowmeter	Mass Flow Sensor with Transmitter	MicroMotion	CMF010P323NRAUEZZZ IFT9701J6N3UR
Pressure Transducer	0-5000psi Thin Film Transducer	Omega Engineering	PX603-5KG5V
PP Containers	Polypropylene Jars, 1200mL& 90mL	Lab Safety Supply	35333, 27783
Filter	316 SS Welded In-line Filter (FW) 0.5µm pores	Swagelok	SS-4FWS-05

Table C-1: List of parts compatible with 98% hydrogen peroxide.

Appendix D

Valve Cleaning Procedure

This appendix describes the procedure that has been used to passivate the valves and prepare them for 98% hydrogen peroxide service in the current heat transfer rig. This procedure is not general and is only valid if the same valves are to be used.

Valves

Swagelok SS-83KS4 (Manual ball valve)
or
Swagelok SS-83KS4-31CD (Pneumatically actuated ball valve)

List of necessary solutions / Lubricants

1. High Strength Ultrasonic cleaner solution
2. Nitric Acid (HNO3), 69.0 - 70.0%, J.T.Baker, 9601-34 [10]
3. Nitric Acid (HNO3), ~35% , obtained by diluting the above solution with deionized water
4. Hydrogen Peroxide (H_2O_2), 30%, J.T.Baker, 2190-236 [10]
5. Hydrogen Peroxide (H_2O_2), 98% HTP, FMC Corporation
6. Deionized water
7. Fluorolube Grease, Gabriel Performance Products, Grade GR-362

Degreasing the Valves

1. Take the valves apart including O-rings and backup rings.
2. Split the valve components into the following 3 containers:
   -1 plastic beaker for the ball, stem, O-ring, backup rings.
   -1 plastic beaker for the valve body.

[10] Ordered from Doe & Ingalls Inc, PO BOX 560, Medford MA 02155-0005.

-1 plastic beaker for the end screws.

3. Clean the O-Rings and the valve body in the ultrasonic cleaner using 50% water-diluted high strength ultrasonic cleaner solution for 2 hours.
4. Clean the end screws in the ultrasonic cleaner using high strength ultrasonic cleaner solution for 2 hours.
5. Rinse all the parts with tap water and scrub with a plastic brush until all lubricant and black sealant is dissolved. (if the black sealant won't come off, see steps 3& 4 of the 316 Stainless Steel component section)
6. Repeat if steps 3 to 5 if necessary.

Passivation of the Valves

1. Split the degreased valves components as follows:
   -1 600mL Pyrex® beaker for all 316 SS and PCTFE coated parts including the ball, the stem, and the seats.
   -1 600mL Pyrex® beaker for all plastics and rubber components: fluorocarbon O-rings, backup rings.
2. Rinse with deionized H2O.

Plastic and rubber components:

3. Immerse with 35% HNO3 for 1 hours at room temperature.
4. Rinse thoroughly with deionized water
5. Condition the parts with 30% H_2O_2 for 12 to16 hours at room temperature. Watch closely for decomposition.
6. Rinse thoroughly with deionized water
7. Final part immersion 98% H_2O_2 for 12 to 16 hours at room temperature. Watch closely for decomposition.
8. Rinse thoroughly with deionized water
9. Air dry and store the parts in a sealed plastic bag

316 Stainless Steel components:

3. Immerse with 70% HNO3 for 30 min at room temperature.
4. Rinse with tap water and scrub the surface with a plastic brush. After this steps the parts should be free of any lubricant and sealant deposits.
5. Immerse with 70% HNO3 for 1.5 - 2 hours at room temperature. (Careful! Part exposure to 70% HNO3 for greater than 2 hours is know to cause galling of the treads)
6. Rinse thoroughly with deionized water
7. Condition the parts with 30% H_2O_2 for 12 to16 hours at room temperature. Watch closely for decomposition.
8. Rinse thoroughly with deionized water

9. Final part immersion 98% H_2O_2 for 12 to 16 hours at room temperature. Watch closely for decomposition, heating of the parts or discoloration of the H_2O_2.
10. If there are no unfavorable results, the parts are considered to be conditioned for H_2O_2 service.
11. Air dry and store the parts in a sealed plastic bag

Reassembly and lubrication of the Valves

1. Wear gloves to avoid contamination.
2. With the fingers, apply a moderate layer of Fluorolube to the backup rings (19), carrier o-rings (20) and end screw seals (21).
3. Place 6 seat springs (17) onto the shank (16).
4. Place other components in order onto the seat carrier: carrier guide (18), backup ring (19), o-ring (20), backup ring (19).
5. Insert the carrier assembly (15-21) into end screws (22)
6. With the fingers, apply a moderate layer of Fluorolube to the ball and stem backup rings and o-rings (7,10,12,13).
7. Reassemble the ball (11) and stem (6); apply a very thin layer of Fluorolube to the ball surface (11)
8. Insert the ball-stem assembly into the valve's body (5)
9. Apply a moderate layer of Fluorolube to the shank PTFE face (15) and a thick layer of Fluorolube on the end screw threads (22). The latter will serve as an anti galling agent for the treads.
10. Insert and tighten evenly the 2 spring loaded end screws assembly (15-22).
11. Keep assembled valves into a sealed plastic bag until ready for use.

Bibliography

[1] Al-Midani, O.M. "Preliminary Design of a Liquid Bipropellant Microfabricated Rocket Engine". Master's Thesis, Department of Aeronautics and Astronautics, Massachusetts Institute of Technology, June 1998.

[2] American Society for the Testing of Materials, "ASTM A380: Standard Practice for Cleaning, Descaling and Passivation of Stainless Steel Parts, Equipment and Systems", website: www.astm.org, 2004.

[3] Bengtsson, E. "The History of Hydrogen Peroxide Propulsion", website: www.peroxidepropulsion.com/article/, 2004.

[4] Bruce, R., Taylor, G. and Taliancich, P. "Ground Testing With High Concentration Peroxide - Lessons Learned", in *22nd AIAA Aerodynamics Measurements Technology and Ground Testing Conference, St. Louis, Missouri*, Paper AIAA 2002-3048, June 2002.

[5] Diez, S. "Preliminary Performance Characteristics of a Microfabricated Turbopump". Master's Thesis, Department of Aeronautics and Astronautics, Massachusetts Institute of Technology, Sept. 2003.

[6] Deux, A. "Design of a Silicon Microfabricated Rocket Engine Turbopump". Master's Thesis, Department of Aeronautics and Astronautics, Massachusetts Institute of Technology, June 2001.

[7] Epstein, A.H. et. al. "Micro-Heat Engines, Gas Turbines, and Rocket Engines: The MIT Microengine Project", in *28th AIAA Fluid Dynamics Conference and the 4th AIAA Shear Flow Control Conference, Snowmass Village*, Paper AIAA-97-1773, June 1997.

[8] Faust, A. "Forced Convective Heat Transfer to Supercritical Water in Micro-Rocket Cooling Passages". Master's Thesis, Department of Aeronautics and Astronautics, Massachusetts Institute of Technology, Feb. 2000.

[9] FMC Chemicals, *Technical bulletin 67: Hydrogen peroxide physical properties*, FMC Chemicals Publication, Princeton, NJ, 1969.

[10] FMC Chemicals, *Technical bulletin 104: Material of construction for equipment in use with hydrogen peroxide*, FMC Chemicals Publication, Princeton, NJ, June 1966.

[11] Jacobson, S. Personal communication, 2004.

[12] Joppin, C. "Cooling Performance of Storable Propellants for a Micro Rocket Engine". Master's Thesis, Department of Aeronautics and Astronautics, Massachusetts Institute of Technology, June 2002.

[13] Kirk, D. Personal communication, 2003.

[14] Lee, J.-W. Personal communication re Ph.D. thesis in progress. Department of Aeronautics and Astronautics, Massachusetts Institute of Technology, 2003-2004.

[15] Lienhard IV, J.H. and Lienhard V, J.H. *A Heat Transfer Textbook*, 3rd ed., Phlogiston Press, Cambridge, MA, 2002.

[16] London, A.P. "A System Study of Propulsion Technologies for Orbit and Attitude Control of Microspacecraft". Master's Thesis, Department of Aeronautics and Astronautics, Massachusetts Institute of Technology, May 1996.

[17] London, A.P. "Development and Test of a Microfabricated Bipropellant Rocket Engine". PhD Thesis, Department of Aeronautics and Astronautics, Massachusetts Institute of Technology, June 2000.

[18] London, A.P., Epstein, A.H. and Kerrebrock, J.L. "High-Pressure Bipropellant Microrocket Engine", *Journal of Propulsion and Power* (July-Aug. 2001), Vol. 17, No. 4, pp. 780-787.

[19] Loppata, J.B. "Characterization of Heat Transfer Rates in Supercritical Ethanol for Micro-Rocket Engine Regenerative Cooling". Master's Thesis, Department of Aeronautics and Astronautics, Massachusetts Institute of Technology, Sept. 1998.

[20] Melof, B.M. and Grubelich, M.C. "Investigation of Hypergolic Fuels with Hydrogen Peroxide", in *37th AIAA/ASME/SAE/ASEE Joint Propulsion Conference and Exhibit, Salt Lake City, UT*, Paper AIAA 2001-3837, July 2001.

[21] MEMSnet, website: http://www.memsnet.org, 2004.

[22] Mok, J.S. et. al. "Decomposition and Vaporization Studies of Hydrogen Peroxide", in *38th AIAA/ASME/SAE/ASEE Joint Propulsion Conference and Exhibit, Indianapolis, IN*, Paper AIAA 2002-4028, July 2002.

[23] Munson, Young, Okiishi, *Fundamentals of Fluid Mechanics*, 3rd ed., John Wiley & Sons, New York, NY, 1998.

[24] Peckner, D. and Burstein I.M., *Hanbook of Stainless Steels*, McGraw-Hill, New York, NY, 1977.

[25] Pinsky, Gu, Covington, and Tucci, "Thermal Hazards Investigation of ≥98% Propulsion Grade Hydrogen Peroxide with Impact on Emergency Relief Design for Safe Shipping and Storage", Presentation Material, FMC Chemical R&D Center, Hazard Assessment Laboratory, Princeton, NJ.

[26] Protz, C.S. "System Analysis of a Microfabricated Storable Bipropellant Rocket Engine". Master's Thesis, Department of Aeronautics and Astronautics, Massachusetts Institute of Technology, Jan. 2000.

[27] Protz, C.S. Personal communication re Ph.D. thesis in progress. Department of Aeronautics and Astronautics, Massachusetts Institute of Technology, 2003-2004.

[28] Schumb, W.C., Satterfield, C.N. and Wentworth, R.L., *Hydrogen Peroxide*, Reinhold Publishing Corporation, New York, NY, 1955.

[29] Shell Chemical Company, *Concentrated Hydrogen Peroxide, Properties, Uses, Storage, Handling*. 2nd edition, Industrial Chemical Division, New York, NY.

[30] Sutton, G.P. *Rocket Propulsion Elements*, 7th ed., John Wiley & Sons, New York, NY, 2001.

[31] Ventura, M. and Mullens, P. "The Use of Hydrogen Peroxide for Propulsion and Power", in *35th AIAA/ASME/SAE/ASEE Joint Propulsion Conference and Exhibit, Los Angeles, CA*, Paper AIAA-99-2880, June 1999.

[32] Yu, D., Warrington, R., Barron, R. and Ameel, T. "An Experimental and Theoretical Investigation of Fluid Flow and Heat Transfer in Microtubes", in *ASME/JSME Thermal Engineering Conference: Volume 1*, 1995.

[33] Yuan, H.S. "Safety & Handling of 90% Hydrogen Peroxide", Presentation given at the Gas Turbine Lab, Massachusetts Institute of Technology, July 2003.

[34] Yuan, H.S. "Thermophysical and Hazards Properties of FMC High Strength Peroxide", Presentation given at the Gas Turbine Lab, Massachusetts Institute of Technology, July 2003.

[35] Yuan, H.S. Personal communication, 2003.